

EXPERIMENTAL ABSOLUTE f-VALUES

for LINES of

Ni, Co, Au, and Ag.

Thesis by

George Melvin Lawrence

In Partial Fulfillment of the Requirements

For the Degree of

Doctor of Philosophy

California Institute of Technology

Pasadena, California

1963

## ACKNOWLEDGEMENTS

I wish to acknowledge the generous encouragement and advice of my thesis supervisor, Professor Robert B. King.

The Office of Naval Research provided financial assistance from June, 1962 to June, 1963.

Mr. John Link and Mr. Robert Ashenfelter have provided valuable aid in the form of illuminating discussions and assistance in the construction and operation of apparatus.

## ABSTRACT

Absolute  $f$ -values are determined for strong lines of Ni, Co, Au, and Ag by the atomic beam absorption method of Bell, Davis, King, and Routly. The equivalent widths of the absorption lines are measured photoelectrically and the density of absorbing atoms in the beam is determined from the beam geometry, kinetic theory, and a microbalance measurement of the atomic beam flux. A comparison is made to existing absolute  $f$ -values and a fit is made to relative  $f$ -values in the literature.

Evidence is presented that the .1-.4 eV states of cobalt are underpopulated in the atomic beam.

A description of the automatic microbalance, the photoelectric scanning system, and an ionization gauge used to monitor the atomic beam is given.

A review of the experimental analysis is given for the purpose of illuminating sources of error and of defining the experimental quantities.

## TABLE OF CONTENTS

|  | Page |
|--|------|
| I INTRODUCTION                                   | 1    |
| II METHOD  | 2    |
| III ANALYSIS                                     | 4    |
| A. Equivalent Width                              | 4    |
| B. Beam Velocity Distribution                    | 5    |
| C. Beam Spatial Distribution                     | 8    |
| D. Boltzman Factors                              | 9    |
| E. Curve of Growth                               | 10   |
| IV EXPERIMENTAL PROCEDURES AND EQUIPMENT         |      |
| A. Beam Density Determination                    | 14   |
| B. Optical System                                | 20   |
| C. Photoelectric Equivalent Width Measurement    | 23   |
| D. Detector Description                          | 30   |
| E. Operational Amplifiers                        | 37   |
| F. Microbalance                                  | 39   |
| G. Atomic Beam Ionization Gauge                  | 43   |
| H. Vacuum, Furnace, Temperature                  | 48   |
| V RESULTS AND COMPARISON WITH OTHER MEASUREMENTS | 49   |
| A. Relative f-values                             | 50   |
| B. Absolute f-values                             | 52   |
| C. Gold and Silver                               | 56   |
| D. Cobalt and Nickel                             | 63   |
| E. Errors  | 78   |

### APPENDIX I

Precision of Atomic f-values and Wavelength Measurements

### APPENDIX II

Photographs

## I INTRODUCTION

An absorption f-value is the number of (classical) electron dipole oscillators per atom needed to explain the strength of an absorption line formed by a group of atoms. A treatment of the theory of the strengths of spectral lines may be found in a text such as the one by Kuhn ( 1 ).

In principle, f-values could be calculated from the atomic wave functions but for the more complex atoms, the theoretical approach is difficult because the answers depend strongly on small variations in the approximate wave functions used. For this reason, experimental f-values are useful for checking approximation methods for wave functions of atoms.

A knowledge of f-values and a measurement of the strength of emission lines has yielded information concerning the density of radiating atoms in sources such as hot gases, plasmas, arcs, and other situations of excitation. In absorption measurements, f-values have found uses in astrophysics, measurements of the density of gases, and spectrochemical analysis.

The measurements of absolute f-values reported herein constitute a continuation and extension of an experiment which has been conducted for several years under the supervision of Professor Robert King. The basic principle of measuring f-values by absorption in an atomic beam was first used by Wessel ( 2 ). The principles, procedures and results of the method as it has been used at the California Institute of Technology have been described by Bell, Davis, King, and Routly (3-7). A recent paper by Professor King (8) comments on the present status of measurements of f-values for neutral atoms in general and on the atomic beam measurements by John Link ( 9 ) and myself. Modifications in the experimental apparatus have been made in order to extend the range of measurement and to facilitate investigation of possible systematic errors.

## II METHOD

Figure 1 illustrates schematically part of the present experimental configuration. A beam of light from a high pressure mercury discharge ( A ) passes through a beam of atoms ( B ) and into the spectrograph entrance slit ( C ). The equivalent widths of the absorption lines are measured by scanning the output of the spectrograph with a photomultiplier, slit, and light chopping system. The density of atoms in the beam is obtained by measuring the deposit rate of atoms on a microbalance pan ( G ) above the furnace, and from a knowledge of the geometrical distribution of the beam and the mean velocity of the atoms as calculated from the temperature of the source. The temperature was measured with an optical pyrometer. In figure 1 the atomic beam effuses upward from a hole in the side of a crucible ( D ) and the beam is made wedge-shaped by the knife edges ( E ). Part of the flux of atoms passes up through the circular aperture ( F ) to the conical balance pan ( G ) where the deposited mass is measured by a recording electrobalance. The manually operated shutter ( J ) under the balance pan is used to control the deposition of mass.

The pressure in the beam area was  $1-4 \times 10^{-6}$  Torr during measurements.

A more detailed description of the photoelectric apparatus, the electrobalance, and of a beam-monitoring ion gauge is given in section IV.

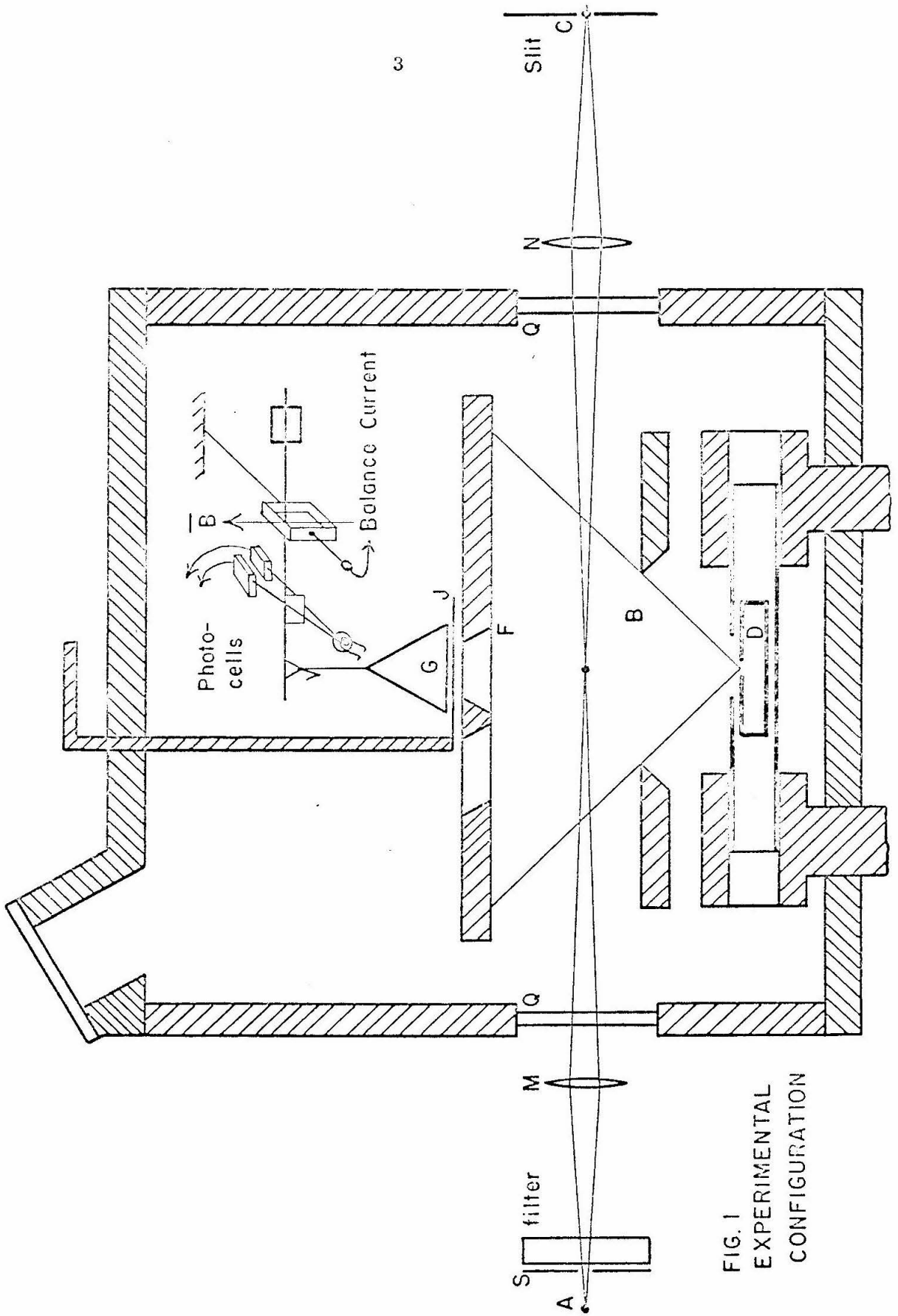


FIG. 1  
EXPERIMENTAL  
CONFIGURATION

## III ANALYSIS

The basic laws governing atomic absorption of light and line formation are described by Unsöld ( 10 ). M. H. Davis ( 3 ) has applied the theory to the situation of absorption in the wide angle atomic beam used in this experiment.

In order to define the experimental quantities used in the analysis of data and to facilitate error analysis, the theory will be reviewed here. For heuristic purposes, an exposition of the theory for absorption in an optically thin atomic beam will be given and then the extension to the case of more dense beams will be stated and described.

## A. Equivalent Width

A source of continuous radiation produces a light beam which passes through a wide-angle atomic beam. Transitions from populated energy states absorb energy from the light beam and later re-emit it in other directions. A small solid angle of the light beam which passes through the atomic beam is studied with the aid of a spectrograph and the amount of absorption is measured. In this experiment, the strength of the absorption line is characterized by the equivalent width measured in wavelength units. This quantity is unchanged by the window curve of the spectrograph. The equivalent width is the wavelength interval of the continuous spectrum which contains the amount of power absorbed from this continuum by the line in question. Thus:

$$W_e = \int \frac{I_0 - I(\lambda)}{I_0} d\lambda, \quad (1)$$

where the integration is taken over the region of the absorption line.

For optically thin absorbers, the equivalent width is given by:

$$W_e = \frac{\pi e^2}{m c^2} f \lambda_0^2 NL ,$$

where  $\frac{e^2}{m c^2}$  is the classical radius of the electron,

$\lambda_0$  is the wavelength of the atomic transition,

$f$  is the (absorption)  $f$ -value which is to be determined, and

$NL$  is the number of atoms per area presented to the light beam from which the energy is absorbed. In equation 1,  $I_0$  is the energy flux per wavelength interval in the continuum and  $I(\lambda)$  is the intensity at wavelength  $\lambda$ .

The value of  $NL$  must be determined in terms of the geometry of the atomic beam, its relation to the position of the light beam, and in terms of the rate of deposit of atoms on the microbalance which is used to measure the atomic beam flux.

## B. Beam Velocity Distribution

Relations between the momentum flux, the particle flux and the volume density of the beam will now be derived. Experimentally, a beam of atoms was produced and the mass flux through a circular aperture above the furnace was determined from the deposit rate on a microbalance pan. The density of atoms was then determined from the mean velocity and the flux. The calculated momentum flux was compared with the observed "impulse" force as a check on the theory and as an aid to understanding the balance tracings.

It is assumed that the atoms of the atomic beam leave the crucible orifice with the spatial and velocity distribution of "Maxwellian effusive flow". This well-known situation is described in texts on kinetic theory. The assumption is made that the atoms leaving the orifice come from an isotropic, Maxwell-Boltzman velocity distribution found in the crucible

at the measured temperature T.

The flux of atoms with speeds between  $v$  and  $v+dv$  at an angle  $\theta$  with respect to the normal to the plane of the crucible orifice is described by:

$$\phi(v, \Omega) dv d\Omega \propto v^3 e^{-\frac{1}{2} \frac{Mv^2}{RT}} \cos \theta dv d\Omega,$$

where  $\phi$  is the particle flux per solid angle, and  $d\Omega = \frac{dA}{r^2}$  is the element of solid angle subtended from the orifice.

R is the gas constant per mole,

M is the molecular weight of the metal, and

T is the absolute temperature of the crucible.

It is implied that the above expression holds only at distances large compared with the diameter of the orifice. The volume density of atoms at speed  $v$  is given by

$$N(v, r, \theta) = \frac{\phi(v, r, \theta)}{v}.$$

Thus, the atoms found in the beam have the same velocity distribution as those in the furnace.

The total flux of atoms of all velocities is

$$\phi(r, \theta) = \int_0^{\infty} \phi(v) dv = \int_0^{\infty} \bar{v} N(v) dv.$$

The total density is

$$N(r, \theta) = \int_0^{\infty} N(v) dv,$$

so that

$$\phi(r, \theta) = \bar{v} N(r, \theta),$$

where  $\bar{v}$  is the average velocity of the atoms in the beam (and in the furnace).

The atoms with speeds between  $v$  and  $v+dv$  carry a momentum

$$P(v, r, \theta) dv dt d\Omega = m v \phi(v) dv d\Omega dt$$

into the solid angle  $d\Omega$  in time  $dt$ .

The total momentum flux is then:

$$P(r, \theta) d\Omega dt = m \bar{v}^2 N(r, \theta) d\Omega dt$$

and is in the direction of  $r$ .

The momentum flux produces an upward force on the pan when the shutter is opened.

Ideally, for a given atom, the ratio of impulse force to deposit rate should be only a function of temperature. This ratio is nominally the time for the balance output to recover the apparent loss in weight after the shutter under the pan is opened. Call this time

$$t = I/gG,$$

where  $I$  is the impulse force,  $g$  is the acceleration due to gravity, and  $G$  is the deposit rate in mass per time. Integrating the momentum and mass flux over the solid angle subtended from the crucible orifice by the circular aperture of diameter  $\frac{2\rho}{\lambda}$  under the balance pan gives:

$$t = \frac{m \bar{v}^2 \int_0^{\tan^{-1} \rho/b} \cos^2 \theta \sin \theta d\theta}{mg \bar{v} \int_0^{\tan^{-1} \rho/b} \cos \theta \sin \theta d\theta},$$

Where  $\rho$  is the radius of the circular aperture under the balance pan, and  $b$  is the distance from the crucible orifice to the plane of the balance orifice.

Evaluation of the integrals gives:

$$t = \frac{\bar{v}^2}{g \bar{v}} \left[ 1 - \frac{1}{4} \left(\frac{\rho}{b}\right)^2 + O^4\left(\frac{\rho}{b}\right) \right]$$

In practice,

$$\rho/b \sim 1/10$$

so

$t = \frac{1}{9} \frac{\overline{v^2}}{\overline{v}}$ , within 1/4%.  
 If  $\overline{v^2}$  and  $\overline{v}$  are appropriate to a Maxwell Boltzman distribution, then we obtain the expression:

$$t = \frac{1}{9} \sqrt{\frac{9\pi}{8} \frac{RT}{M}}$$

### C. Beam Spatial Distribution.

The light beam is considered to be a ray which passes horizontally through the atomic beam at an elevation  $Z_0$  above the crucible orifice. Copper knife edges are used to make the atomic beam wedge shaped with a half angle  $\chi$ . The optical density of atoms, NL is given by

$$NL = \int N(x) dx,$$

where the integration is performed along the path of the light ray. To calculate NL, let us perform this integration for a horizontal ray passing perpendicular to the knife edges and through the vertical line from the crucible orifice. We want also to relate NL to the mass arrival rate G at the balance. Thus,

$$\frac{NL}{G} = \frac{\int N(x) dx}{\int m \phi(r, \theta) d\Omega},$$

Where m is the mass of the atoms, the integration in the numerator is performed along the path of the light ray, and the integration in the denominator is made over the solid angle subtended by the circular orifice under the balance pan. Taking as coordinates

$$d\Omega = 2\pi \sin\theta d\theta; \quad \chi = z_0 \tan\theta$$

the expression becomes

$$\frac{NL}{G} = \frac{\int_{-\delta}^{\delta} \frac{\cos \theta}{(z_0 \sec \theta)^2} z_0 \sec^2 \theta d\theta}{m\bar{v} \int_0^{\tan^{-1} \rho/b} 2\pi \cos \theta \sin \theta d\theta}$$

Integration gives

$$\frac{NL}{G} = \frac{2 \sin \delta}{m\bar{v} \frac{\pi \rho^2}{b^2 + \rho^2} z_0} \quad (2)$$

Then, since

$$W_e = \frac{\pi e^2}{mc^2} f \lambda^2 NL,$$

we obtain

$$W_e = \frac{\pi e^2}{mc^2} f \lambda^2 \frac{G}{\bar{v}} \frac{2 \sin \delta}{\frac{\pi \rho^2}{b^2 + \rho^2} z_0}, \quad (3)$$

which enables the calculation of  $f$ , for optically thin beams, from the experimental data and known parameters.

#### D. Boltzman Factors.

The mass deposit rate  $G$  is properly the arrival rate of those atoms which were in the lower state of the observed transition when the atoms passed upward through the light beam. For energy levels  $E_i$ , we would expect the atoms to have a Boltzman distribution:

$$G_i = G \frac{g_i e^{-E_i/KT}}{\sum_j g_j e^{-E_j/KT}}$$

where  $G_i$  is the deposit rate of atoms in the  $i^{\text{th}}$  state,  
 $G_{\text{total}}$  is the deposit rate of all atoms on the balance, and  
 $g_i$  is the statistical weight of the  $i^{\text{th}}$  state.

This distribution certainly can be expected to hold inside the crucible where the temperature is  $T$  but there is evidence that the higher energy states ( $E_i > kT$ ) become somewhat depopulated as the beam leaves the crucible orifice. This problem occurs with the cobalt transitions from the  $b^4F$  terms and will be discussed in section VD.

#### E. Curve of Growth .

The way in which the equivalent width increases with increasing NL is called a curve of growth. Davis (3) has shown that for lines with a single, Doppler-broadened component, equation 3 generalizes to the curve of growth:

$$\frac{W_e}{\Delta \lambda'_D} = \sqrt{\pi} \sum_{n=1}^{\infty} \frac{(-1)^{n+1} C^n}{n! \sqrt{n}} \quad (4)$$

where the beam velocity distribution has been assumed to be Maxwellian, and

$$\Delta \lambda'_D = \frac{\lambda_0}{c} \sqrt{\frac{2RT}{M}} \sin \delta$$

is the usual Doppler width multiplied by  $\sin \delta$ , and  $C$  is defined as :

$$C = \frac{\pi e^2}{mc} \frac{\lambda_0 f}{\sqrt{\frac{2RT}{M}}} \frac{2}{z_0 \pi} G \frac{b^2 + \rho^2}{\rho^2} \frac{1}{\sqrt{\pi} \bar{v}} \quad (5)$$

Note  $C \propto \frac{NfL}{\Delta \lambda'_D}$  ,

and for  $C$  sufficiently small, equation 4 becomes:

$$\frac{W_e}{\Delta \lambda'_D} = \sqrt{\pi} C \quad (6)$$

The non-linear function defined in equation 4 is the Doppler curve of growth described by Unsöld ( 10 ) and others, except that  $\Delta \lambda_D$  is replaced by  $\Delta \lambda_D \sin \delta = \Delta \lambda'_D$ . To facilitate the reduction of the experimental data, numerical tables of the quantity C as a function of  $W_e / \Delta \lambda'_D$  were used to obtain a value of C and thus f from the measured equivalent width and temperature. For most of the data used in determining the f-values, the curve of growth calculation gave f-values differing less than 10% from the values given by the linear approximation, equation 6.

Once a value of C was determined corresponding to a given measurement of  $W_e$ , the f-value could be calculated from:

$$f = QCT/G$$

where

$$Q = 3.28 \times 10^{-3} \frac{\rho^2}{\rho^2 + b^2} \frac{Z_0}{\lambda_0}$$

$\lambda_0$  in  $10^{-5}$  cm.  
 $Z_0$  in cm.

The quantity Q depends on the geometry of the furnace and the wavelength and thus is constant during a run on one line.

Of the metals Au, Ag, Ni, and Co, the Doppler curve of growth defined in equation 4 can be strictly applied only to nickel. This is because nickel exhibits no hyperfine structure.

In a qualitative sense, hyperfine structure broadens the basic line profile. This means that the absorbed energy is removed from a larger range of wavelengths and thus requires more atoms to produce saturation, extending the range of the linear portion of the curve of growth.

It is difficult to obtain exact expressions describing the curve of growth for lines split into hyperfine components but approximations of sufficient precision can be obtained for use with weak absorption lines.

One situation in which the curve of growth can be exactly modified to include the presence of hyperfine structure is the situation where the hyperfine components are separated by a distance larger than the Doppler width. The  $i^{\text{th}}$  hyperfine component will contribute partial equivalent widths  $W_{ei}$  which will each follow a curve of growth:

$$\frac{W_{ei}}{\Delta \lambda'_D} = \sqrt{\pi} \sum_{n=1}^{\infty} \frac{(-1)^{n+1} (C_i)^n}{n! \sqrt{n}}$$

where  $C_i$  is proportional to  $p_i$  with  $p_i$  the fractional intensity of the  $i^{\text{th}}$  component. That is,

$$\sum_i C_i = C, \quad \sum_i p_i = 1, \quad C_i = p_i C \quad \text{and} \quad \sum W_{ei} = W_e$$

The last five equations define a composite curve of growth which describes the relation between the total equivalent width of the line and the value of NFL for separated, Doppler broadened hyperfine components. The composite curve of growth formed by splitting  $C$  in this manner was plotted on a graph so that values of  $C$  could be obtained for each experimental value of  $W_e/\Delta \lambda'_D$ . If the hyperfine components have equal intensities, then the splitting of  $C$  into equal components gives partial equivalent widths that are equal. Splitting  $C$  into unequal components produces a composite curve of growth which saturates less rapidly than a curve of growth obtained by splitting  $W_e$  in the same, unequal, proportions.

The elements Co, Au, and Ag exhibit hyperfine structure that is not easily characterized by separated, Doppler broadened components. To obtain values of  $C$  from the measured equivalent widths for a line, a consideration of the hyperfine structure was made and a choice of a method for obtaining a curve of growth was decided upon.

The hyperfine structure of the Co, Au, and Ag lines and the curve of growth modifications for each will be discussed in sections V, C and D.

Information concerning the existence and extent of the hyperfine splitting was obtained from the tables of Landolt-Bornstein ( 11 ).

#### IV EXPERIMENTAL PROCEDURES AND EQUIPMENT

##### A. Beam Density Determination

Figure 2 shows portions of two recordings of the microbalance output as a function of time. Time increases toward the left and mass increases toward the top. At the right hand side, the shutter under the pan is closed and the balance output is constant within  $1/2$  microgram. Then the shutter under the pan is opened and the upward momentum of the beam (impulse force) lightens the pan and the atoms begin depositing and causing the indicated mass to rise with time. Generally, the shutter was operated so as to record the mass flux during the time when the absorption line was scanned. At the left-hand side of figure 2 the shutter was closed and the balance registered an increase in weight.

Nominally, the deposit rate  $G$  is given by the slope of the rising portion of the recording. In the processing of the chart paper from a run, a best straight line was drawn through the deposit record and the slope of this line taken as the deposit rate.

The slope, however, is not only the rate of mass increase, but is the sum of the rate of mass increase and the rate of impulse force decrease. For each record the impulse force was measured from the shift in the chart recording upon closing the shutter. If the impulse force was found to be changing linearly with time over a period of a half an hour or so, the rate of change of the impulse force was used to correct the balance slope to give a true deposit rate. About one fifth of the data were corrected this way and the amount of correction did not exceed 10%.

The values of impulse force constitute quantitative data that can be used as a check on the beam velocity distribution and on the deposition

mechanism. For each element, values of impulse force obtained at the closing of the shutter were plotted versus the corresponding value of the deposit rate  $G$  and the points were compared with the theoretical value of the impulse force,  $tG$ . An example of such a plot is shown in figure 3 for some of the nickel data. Because increases in  $G$  are obtained by increasing the temperature  $T$ , the theoretical value of the impulse force is a slightly non-linear function of  $G$ . It will be noted that on the average, the observed values of the impulse force agree with the predicted values within a few percent. The ratio of the measured impulse force to the measured deposit rate was taken as an experimental value of the recovery time  $t$ . The average ratio between the experimental recovery time and the expected recovery time (section III B) was found to be  $1.01 \pm .02$  for Ni, Co, and Ag. The average for Au was  $1.03 \pm .01$ .

Almost invariably, the impulse force obtained when opening the shutter was one or two micrograms larger than that obtained upon closing the shutter. This effect was traced to gassing and degassing of the microbalance pan caused by temperature changes. The action of a hot furnace without a crucible was investigated. It was found that the radiation from the furnace would cause a decrease in mass of the pan of one or two micrograms in the course of 30 seconds and upon closing the shutter the mass recovered in about a minute. At the left hand end of the upper tracing in figure 2 the recovery of the mass is evident. A light bulb placed near the pan as a heater could be made to produce the same amount of outgassing and gassing. During runs, the light bulb was turned on near the pan to help reduce the gas capacity of the pan. In the recording and measuring of the records, the shutter was left open long enough to obtain a record of deposit rate after the pan had reached a constant temperature. This meant allowing the shutter to

be open for at least two minutes.

At the pressures of  $2-4 \times 10^{-6}$  Torr attainable in the beam area, the impact rate of residual gas particles upon the balance pan is approximately the same as the arrival rate of atomic beam atoms. This naturally leads to the question of how much of the measured deposit rate corresponds to metal beam and how much to occlusion of gas during the deposition.

Greiner, Yetter, and Gleason ( 12 ) at the IBM laboratories have made a mass spectrometer study of the amount and composition of gas occluded in vacuum deposited nickel films. These workers evaporated films under varying conditions which included: Pressures from  $10^{-4}$  to  $10^{-6}$  Torr, with and without liquid nitrogen cold trapping of the oil diffusion pump, and at various deposit rates. At conditions similar to those of this investigation, they found a concentration of less than .1% gas atoms per nickel atom in the deposit. The occluded gas consisted of roughly equal parts of hydrogen and carbon monoxide. At  $10^{-4}$  Torr and without cold trapping, the gas content of the film was as high as 1%. Because of the small amount of gas detected by Greiner, Yetter and Gleason, it was concluded that occlusion of gas would contribute a negligible error in the determination of beam density.

In the computation of the f-values reported in this experiment, no corrections have been made for the effect of atoms reflecting from the microbalance pan. The fraction of condensable particles impinging upon a surface that stay on the surface is called the sticking coefficient. The value of the sticking coefficient depends upon the particle and upon the surface, the history and condition of the surface, and on the amount of particle flux. A review article on the subject has been written by Wexler ( 13 ). Generally

speaking, metals condensing on the surface of a dissimilar metal have a sticking coefficient of .1 to .8, while the sticking coefficient for metallic beams upon freshly deposited surfaces of the same metal have a range of about .8 to 1. The reflection or non-sticking of atoms is found to occur diffusely and can more descriptively be called a re-evaporation rather than a reflection.

To help trap all atoms passing up through the balance orifice, the balance pan was made in the form of a cone. These cones were made of .00025 inch aluminum foil and had a half angle of about  $10^{\circ}$ . The half angle of the cone was such that if an atom re-evaporated from a position near the apex of the cone, there was approximately a 2% chance that it would leave the cone without making a further encounter with the wall. It was estimated that the pan collection efficiency for the atoms under investigation should be at least 99%.

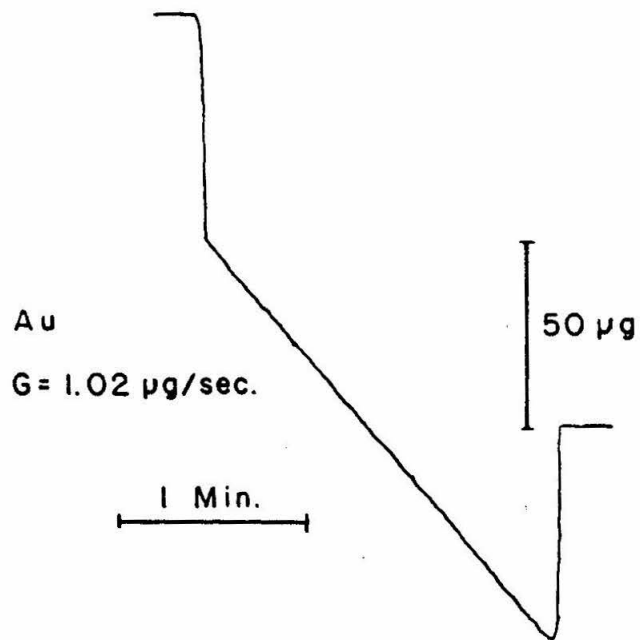
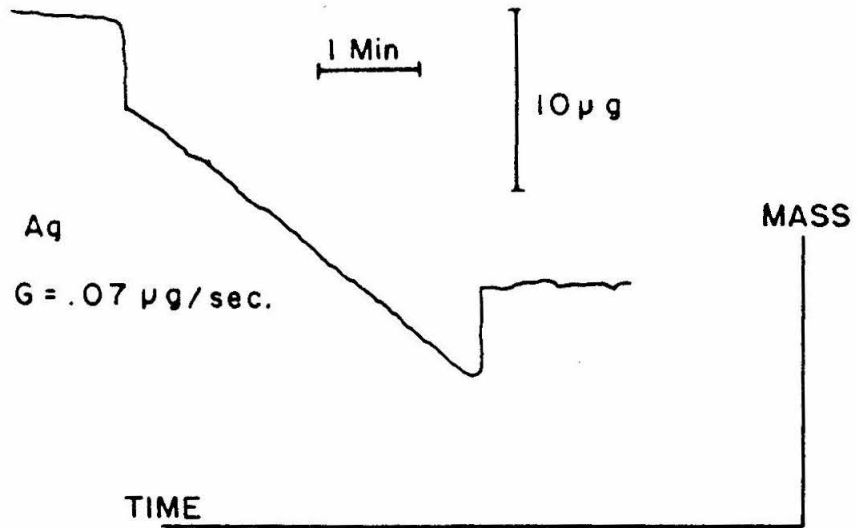
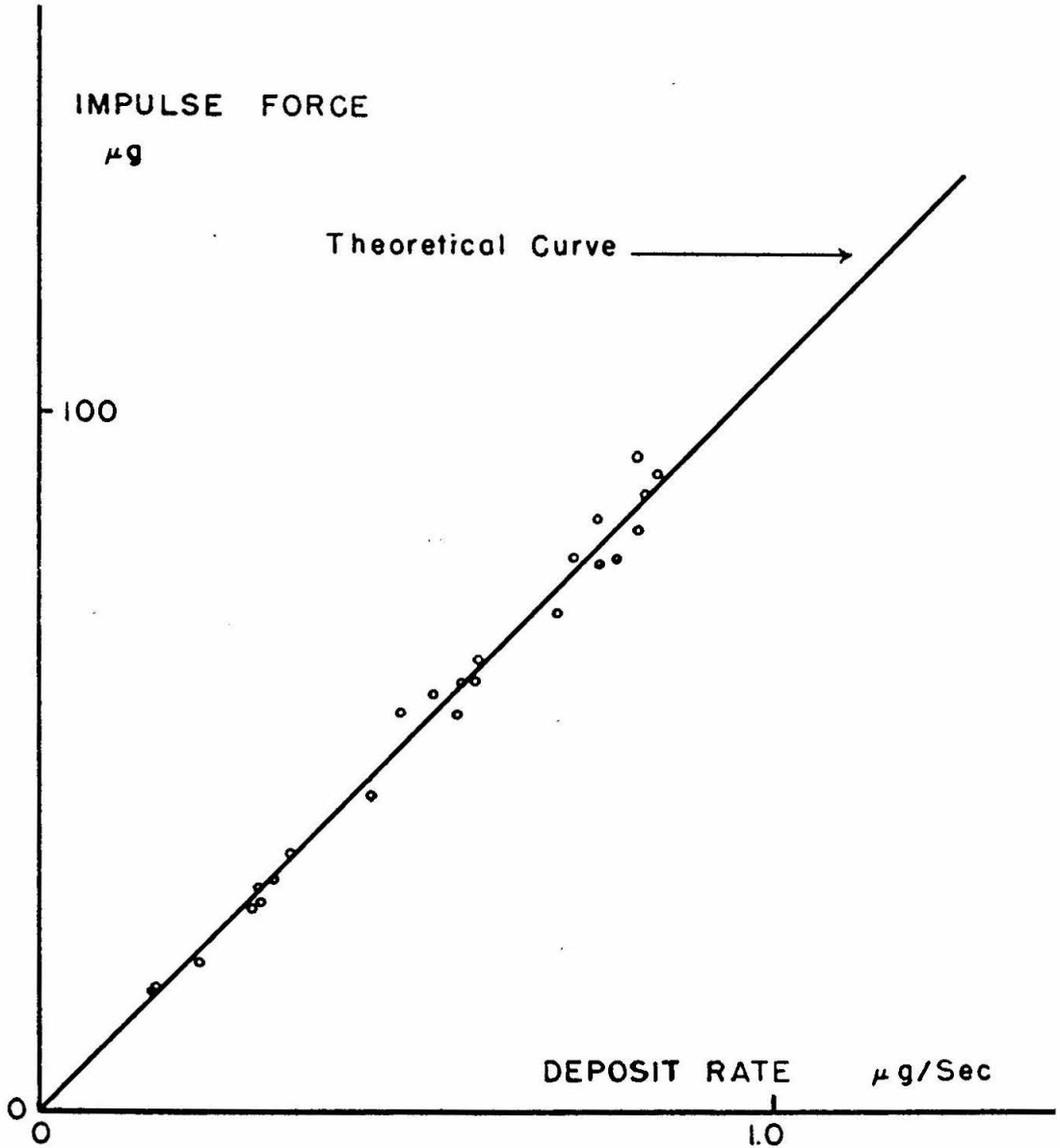


FIG. 2 BALANCE RECORDS

FIG. 3 NICKEL IMPULSE FORCE  
versus DEPOSIT RATE



## B. Optical System

The part of the optical system from the light source to the spectrograph entrance slit is illustrated schematically in figure 1. A high pressure mercury discharge lamp ( A ) is the (horizontal) line source which is imaged in the center of the atomic beam and again at the spectrograph entrance slit ( C ). Elements ( M ) and ( N ) are the quartz lenses with focal lengths 15 and 25 cm. respectively. The stop ( S ) is a black plate with a 1/4 inch diameter hole placed around the (much smaller) image of the spectrograph grating. This protects the operator of the equipment from sunburn and reduces unnecessary excitation of the atomic beam by light other than that which passes through the spectrograph. The quartz windows ( Q ) are sealed to the vacuum system with O-rings. The filter was used to eliminate the first order spectrum and to eliminate any visible scattered light. For the Au line 2428, a liquid filter was used. This filter is described by Strong, pg. 363, ( 14 ) and transmits from  $2300 \text{ \AA}^{\circ}$  to  $2800 \text{ \AA}^{\circ}$  but is opaque in most of the visible region of the spectrum. For all other lines, the filter was a Corning glass filter no. 7054 "Red-purple Corex A". This filter passes ultra-violet and deep red. The phototube is blind to the red which is passed.

The limiting apertures in the optical system are in the spectrograph. The bundle of rays which pass through the atomic beam fairly well approximates a single ray as called for in the analysis. At the places where the light beam enters and leaves the atomic beam, the light beam is about .1 inches thick in the vertical direction. The elevation of the light beam above the furnace (  $Z_0$  ) was determined by noting the decrease in intensity of light reaching the photomultiplier as a depth micrometer rod was lowered into the bundle of rays passing through the furnace. This measurement gave a value of  $Z_0$  that was well defined and reproducible to better than 1/2%.

During most of the measurements the value of  $Z_0$  was about 1 1/2 inches.

The photocurrent due to scattered light under the conditions of operation was estimated to be 2 nanoamperes in the presence of a "true" current of 1000 nanoamperes. At the Au line  $\lambda 2428$ , however, the total current was only 3 nanoamperes and so measurements there must be corrected for the scattered light actually present. ( See section V,C )

The light source was a high pressure mercury quartz capillary discharge. This lamp is a PEK labs type A with a quartz water jacket. It was water cooled with tap water and operated at about 1kv. and 1 amp. DC. The discharge operates at a few hundred atmospheres pressure and the mercury lines are highly broadened. The spectrum was measured photoelectrically in this laboratory as a guide to equipment adjustment and was found to be quite similar to that of the General Electric company's lamps described by Stahl ( 15 ). In the visible and near ultraviolet region of the spectrum, the mercury peaks have a half width of about fifty Angstroms and there is a pseudo-continuum between peaks that is about one fifth the intensity of the peaks.

The lamp intensity was found to vary ( usually decrease ) as much as ten percent in the course of an hour. Some of the causes of this were variations in cooling water pressure and contamination of the water jacket by tap water.

The shape of the spectrum is voltage dependent. This means that the photoelectric scanning system, which obtains reference signal from a different wavelength than the line under investigation, will show noise in response to some types of lamp fluctuations. This was found to be troublesome only in the cases when the scanner was located on a rapidly changing part of the spectrum, such as near the peak of a mercury line.

Of interest in the operation of the lamp is its DC volt-amp characteristics. Below about 550 volts the lamp behaves much like a resistance of 250 ohms. At 550 volts a transition in characteristics takes place and the lamp operates at a nearly constant current of about one ampere up to the point when the lamp is destroyed at about 1500 volts.

A ballast resistance of 250 ohms was used in series with the lamp and the motor generator supply. To start the discharge, the supply voltage was set at 500 volts and the high voltage terminal excited with a leak detector Tesla coil. After the lamp started, the voltage was increased to 1000 or 1100 volts.

### C. Photoelectric Equivalent Width Measurement

The method of equivalent width measurement formerly used in this atomic beam experiment was to photograph the absorption spectrum, calibrate the photographic plates and then scan the absorption lines with a microphotometer.

In the present form of the experiment, the photographic plate was eliminated and, in effect, a microphotometer was constructed on the focal curve of the spectrograph.

Such a course of action was motivated by a desire to measure smaller equivalent widths than previously possible and to eliminate the photographic calibration. Using the photoelectric method, measurements were made of equivalent widths as small as  $.3m\text{\AA}^0$ . The ability to measure small equivalent widths makes it possible to determine  $f$ -values from data taken on the linear portion of the curves of growth. In the cases where there is considerable blending of the Doppler broadened hyperfine components of a line, the shape of the curve of growth for  $W_e/\Delta\lambda_D'$  greater than, say, .6 is not well known. If other factors are constant, the extension to smaller  $W_e$  makes smaller values of  $Nf$  available for measurement.

In addition to the elimination of photographic grain noise, the greater photon efficiency, and the elimination of the need for calibration, further conveniences were realized by the presence of a phototube monitoring the output of the spectrograph. Focussing of the optical system in the ultra-violet region of the spectrum was aided by using the photomultiplier current as a sensor. The geometry of the light beam was studied and measured with the help of the photocurrent. Loss of light intensity with time caused by contamination of the lamp water jacket and from condensation of metal atoms on the furnace windows was monitored by the phototube.

Phototubes have a much wider dynamic range than a photographic plate and therefore the problem of determining the correct exposure time is eliminated. This meant that absorption lines which occurred on the edge of peaks of the mercury lamp spectrum were measurable.

Two methods of obtaining equivalent widths photoelectrically were considered. One method was to place the absorption line completely within a wide slit and measure the fractional change in the light intensity when the absorbing atomic beam was produced. The equivalent width would then be given by the product of the slit width (in wavelength units) and the fractional change in intensity. The method chosen, however, was to scan the line shape at a constant speed with a very narrow slit and then planimeter the area of the line profile. It was felt that the scanning method would be more free of systematic errors and exhibit a higher signal to noise ratio than the wide slit method.

A light chopping system was used to reduce the effect of variation in light source intensity and photomultiplier gain.

The lower limit of equivalent widths that can be measured is determined by the noise level of the photomultiplier current that measures the light intensity and by the accuracy with which small changes in this intensity can be measured. Changes in intensity as the line was scanned were recorded on a chart recorder, by recording the difference between the current from the line's wavelength,  $\lambda$ , and a reference current obtained from a nearby wavelength,  $\lambda'$ , in the continuum.

Figure 4 shows schematically how this was done. Two slits separated a distance of .2 inches are located at the focal surface of the spectrograph. A reciprocating shutter driven by a cam allows light to

pass to the photomultiplier tube cathode through each slit alternately in time. The width of the shutter aperture is adjusted so as to give about 10% dark time. The position of the shutter aperture with respect to the slits and the cam is arranged so that each slit is open for an equal time. A synchronous SPDT switch attached to the shutter switches during the dark time and separates the photomultiplier output current into two separate signal channels. The average current in one channel is then proportional to the intensity at wavelength  $\lambda$ , and the current in the other is proportional to the intensity at wavelength  $\lambda'$ . The DC component of the current in each channel is then made available for recording with the help of two operational DC amplifiers and RC filters.

A meter or chart recorder was connected from the reference output to the signal output to measure or record the difference between the two. Just before scanning lines, the reference slit was adjusted in width so that the current in the reference channel was one or two percent more than the current in the signal channel.

As the line was being scanned by moving the scanner carriage along the focal curve of the spectrograph, the Brown chart recorder was connected between the output of the two amplifiers and recorded the difference between the signal and reference currents on a convenient scale. Once every minute, a timer briefly switched the chart recorder input to record the value of the signal current. The resulting record then contained the value of the (sampled) signal current and the variations in the signal current magnified by a known scale ratio. An example of such a record is shown in figure 5. To obtain the equivalent width, a baseline was drawn between the continuum levels on each side of the line and the area of the line was measured with a planimeter. The equivalent width was

obtained by dividing the area of the line by the value of the continuum current multiplied by scale factors having to do with the chart speed, the scanning velocity, the spectrograph dispersion, and the scale ratio between the signal current and the difference signal.

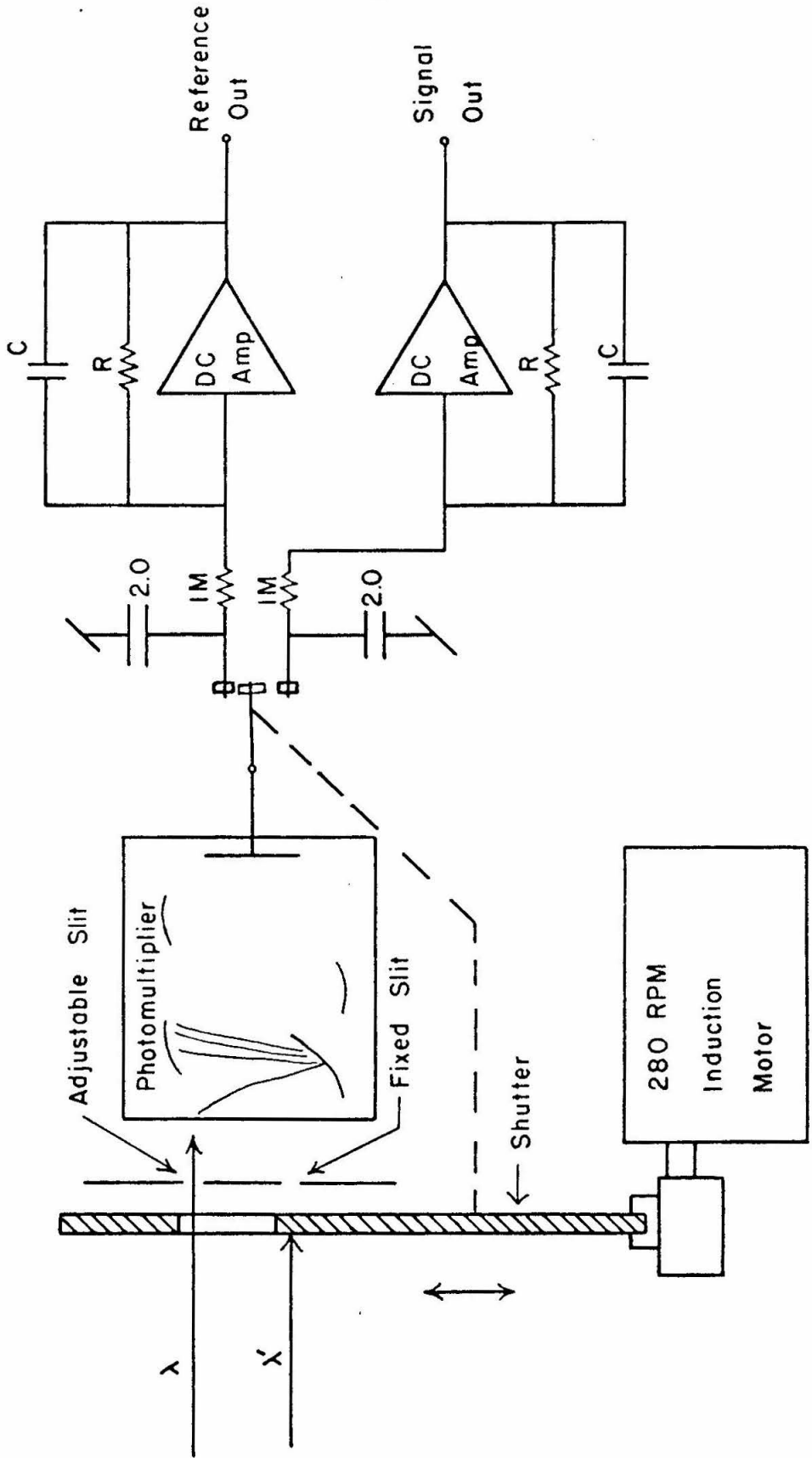


FIG. 4 LIGHT CHOPPER and Detector System

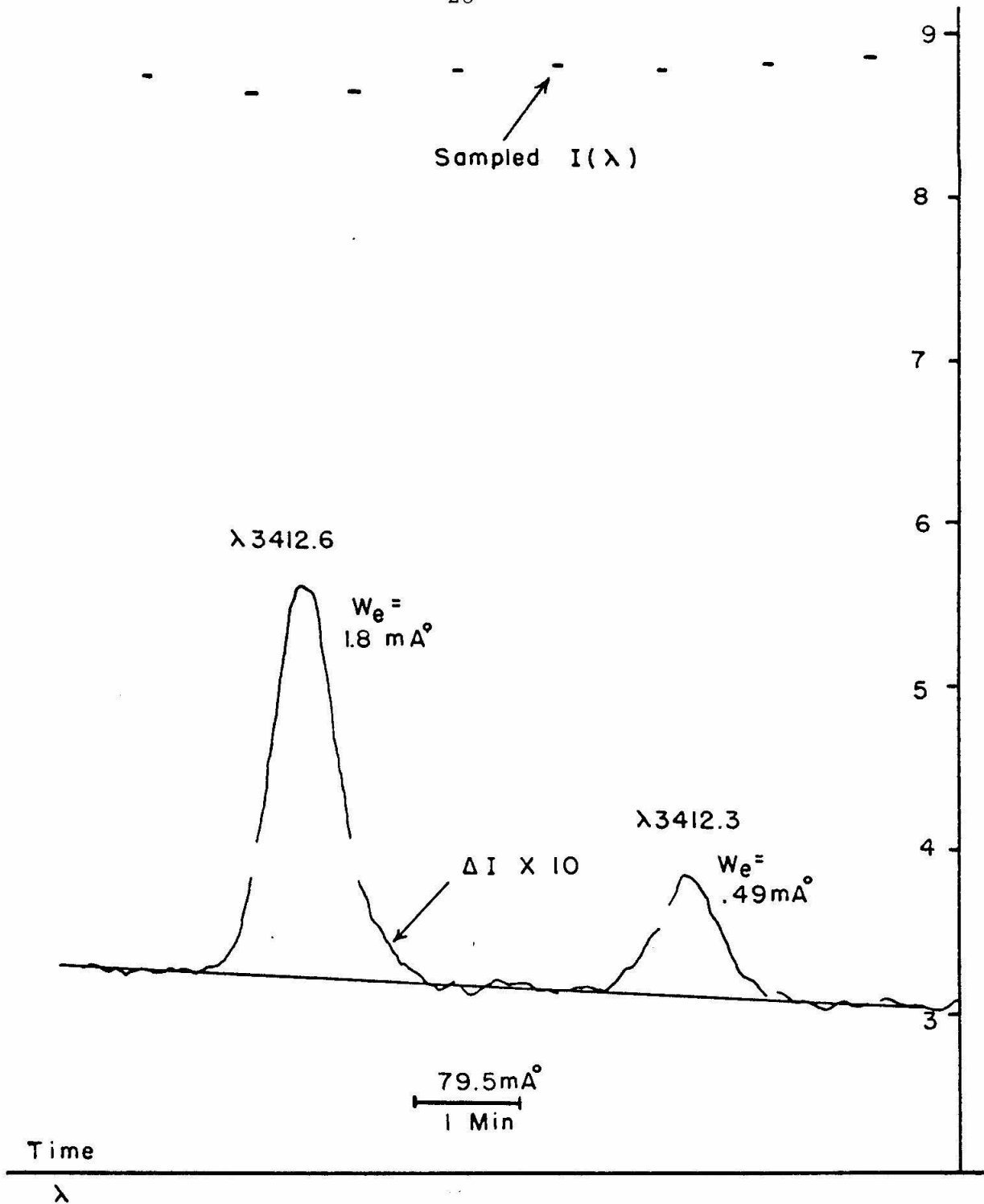


FIG. 5 PHOTOCURRENT  $\Delta I \times 10$  AND  $I(\lambda)$

SCAN 8 Co  $\lambda 3412.34$  AND  $\lambda 3412.63$

To determine the equivalent width by measuring the chart recording of the line with a planimeter, a baseline representing the value of the continuum intensity must be determined. This was done by drawing a straight line connecting the portions of the continuum on either side of the line profile. This method assumes that the difference signal is a linear function of wavelength in the region of the line and that no malfunction of the chopper occurred during the scan to artificially shift the difference signal. Because of noise in the difference signal, a long baseline (long scan time) increased the accuracy of the determination of the continuum intensity. Most scans were five or six minutes in duration, equivalent to a distance of 400 to 480  $\text{m}\text{\AA}$  in second order.

Since the measurement of  $W_e$  depends on finding the area of small perturbations in the photomultiplier current, the experiment requires as small a noise as possible in the photocurrent. The precise measurement of a given light intensity is limited by the production of the photocurrent in discrete quanta, the photoelectrons. The observed noise in the photocurrent consists partly of a constant percentage introduced by the chopping process and other sources and of another part proportional to the square root of current. At currents below .1 microamp the noise in the system is contributed largely by photoelectron statistics, and above a current of 1/2 microamp, the statistical noise is less than that contributed by other sources.

Generally, no significant noise was attributable to fluctuating phenomenon in the light source. Measurement showed that when the lamp intensity was changed by 10% of its value, the difference signal changed by 10% as expected and not by the change in the total intensity.

Erratic jumps of one percent or so in the value of the difference signal could be eliminated by adjustment and cleaning of the synchronous switch. Small irregularities in the cam bearing and therefore in the cam motion seem to be the most probable cause of the residual .2% noise. This was reduced somewhat by the use of a high tolerance ball bearing to support the cam shaft. This source of noise could, in principle, be reduced either by improving the precision of the shutter mechanism or by measuring only the Fourier component of the photocurrent at the chopping frequency instead of the difference of the DC signals. The amplitude of the fundamental component is less sensitive to variations in the ratio of the times that the two slits are open than is the DC value of the difference signal.

The nature of the baseline noise can be seen in figure 5.

#### D. Detector Description

Figure 14 in appendix II is a photograph of the chopper-slit-phototube assembly mounted in the spectrograph plate holder. This assembly (called the "carriage" by its users) is driven along the focal curve of the spectrograph by an oversize micrometer head. This "heavy-duty" Starret no. T465 micrometer has a screw approximately one half inch in diameter with a pitch of .025 inches. The thimble is calibrated in ten-thousandths of an inch. The nut of the micrometer was fastened to the carriage frame and the screw and thimble were driven at 1/10 rpm. The micrometer drive consisted of a 3 rpm reversible synchronous motor driving a thirty to one worm reduction gear. The worm gear shaft rested upon a ball thrust bearing. The worm gear shaft and the micrometer screw were coupled with a bellows coupling containing two steel balls separated by a rod. This arrangement allowed a certain amount of play perpendicular to the axis of rotation but provided a non-

backlash torque transfer and prevented axial play.

The speed of rotation of the micrometer thimble was found to be constant to better than one percent over periods of a minute -- the approximate time required to scan absorption lines. The carriage motion as a function of micrometer reading was investigated by measuring the motion of the carriage with a good quality dial indicator with divisions every .0005 inches. This measurement indicated that the scan speed was known and constant to 4% or better.

To check the effect of velocity variations, a strong absorption line formed by silver in a quartz absorption cell held at constant temperature was scanned several times, alternately up and down the plate holder. The mean deviation of the equivalent widths obtained was 5% and there was no significant difference between the up and down directions. A further check and precaution was taken. Lines were scanned using different portions of the micrometer screw. Again, no significant systematic difference was found.

Some data, however, had to be rejected because of difficulties with the scanner. For example, during the scanning of nickel lines on Feb. 21, 1963 the bellows coupling between the three rpm motor and the worm gear broke in such a way as to cause intermittent rotation of the drive screw. The trouble was found and the appropriate data rejected. It was also found that if the brass strips which held the carriage onto the track were tightened too much, a systematic difference appeared between the equivalent widths obtained scanning up and down.

A generous estimate of the systematic error in  $W_e$  contributed by the variations and errors in scanner speed is about five percent. The scatter in  $W_e$  values was somewhat larger and can be attributed to variations in beam geometry and beam density and to base line noise.

The photomultiplier tube used was a type 9526 B made by EMI-US corporation. It has an end-on quartz window and its spectral response extends to  $2000\text{\AA}$  in the ultra-violet. The particular tube used (Serial no. 5916) had a dark current of less than one nanoampere at room temperature and thus required no cooling or correction for a constant offset current in most of the measurements made.

The photomultiplier was mounted on top of the scanner carriage block with the photocathode window facing the two slits. The tube was set in a brass housing and wrapped in magnetic shielding material. The housing was equipped with air connections to provide for cooling by cold, dry air if necessary to reduce dark current.

The resistance divider for the dynode voltages was assembled on the teflon tube socket and carried 300 microamperes at 1200 volts cathode-to-ground voltage. The cathode-to-first-dynode voltage and the anode-to-ground voltage were set at twice the dynode voltages.

The power supply for the photomultiplier was a Model 420M made by the John Fluke Company. The manufacturer specifies a regulation of .01% in the output voltage.

The reciprocating shutter indicated in figure 4 is driven by a cam turning at 280 rpm. The cam is made of polished drill rod set .1 inches off center and operates the spring loaded shutter by sliding on a nylon pad attached to the edge of the shutter. The shutter motion is thus sinusoidal with a period of  $4 \frac{2}{3}$  cycles per second and with an amplitude of .1 inches. The shutter aperture is equipped with adjustable edges so that the switching waveform can be changed. In general, the signal and reference channels were set to be open an equal amount of time and the dark time was set at 10%.

The sliding parts of the chopper mechanism were lubricated with "Lubriplate".

Since the ratio of the signal current to the reference current is proportional to the ratio of time the signal slit is open to the time the reference slit is open, it is important that the motion of the shutter is the same from cycle to cycle. If the chopper had been turned off for some time, it was found that the above ratio would drift as much as five percent in a two hour period after the shutter drive motor was turned on. This effect could be explained by a plastic flow of the nylon cam pad in such a way as to shorten the distance between the cam shaft and the shutter aperture. The effect was not serious and could be eliminated by running the chopper a few hours before a run.

Random variations in the motion of the shutter were certainly responsible for some of the noise in the difference signal. (See pg. 30.)

The carriage used for scanning the spectral lines is shown schematically in figure 5 and photographically in figure 14 in appendix II. The carriage contains the photomultiplier, slits, chopper shutter, synchronous switch, chopper motor, and the micrometer drive screw. The carriage framework was machined from an aluminum block and the shutter was made from sheet aluminum. The aluminum parts were anodized black to reduce stray light and to provide a hard surface for the sliding action.

The two slits were mounted on a cylinder installed in the carriage frame in such a way as to provide rotation of the signal slit about its center. This allowed the signal slit to be aligned parallel to the image of the spectrograph entrance slit. This rotation alignment was most easily done by peaking the photomultiplier output in response to the light from a convenient emission line, say from a mercury lamp.

Fixed slits were made from "Gillette Super Blue Blades". Microscopic examination revealed that the edges of the blades had nicks less than one micron in size but two typical edges would form a slit whose width varied at least five microns along its length. To correct this lack of straightness, the edges of the blades were ground by hand with number 600 carborundum and water on a piece of flat glass until two parallel edges were produced. These ground razor blade edges were cemented to a small aluminum or brass block machined to pass the light and hold the slit edges. One edge of the block was undercut to provide an edge of the adjustable reference slit. Several slits were made and their widths measured on a comparator. Most of the lines were scanned with a slit approximately 15 microns wide. (The entrance slit of the spectrograph was set at 30 microns width.)

The synchronous "detector" switch in figure 6 and in figure 14 of appendix II consists of a set of ordinary SPDT silver-alloy relay contacts mounted so as to be operated by the shutter motion. The contacts were rounded and polished. Set screws adjust the amount of travel of the center contact. Reliable operation can be obtained with as little as .002 inch travel. The shutter itself travels .2 inches and the extra motion is absorbed by the flexing of a beryllium copper extender arm silver soldered to the center leaf. Because of the short switching distance compared to the shutter stroke, the time of electrical switching can be easily set to occur within the dark time. This prevents any contact bounce from producing noise in the difference signal. The timing of the switch was adjusted by rotating the switch assembly around its mounting screw. The adjustments of the switch were made while watching the photomultiplier current waveform on an oscilloscope. Figure 6 shows the circuit used to facilitate adjustment of the switch and the idealized oscilloscope waveforms. The battery supplies a negative bias current, the absence of which produces a marker pulse while the switch is traveling between contacts.

It is very important that the two outside switch contacts never contact the center arm at the same time. Such a shorting equalizes the voltage on the 2 mfd input filter capacitors and drives the difference signal to zero. If shorting occurs during occasional cycles, the difference signal shows erratic behaviour. If the switch is permanently shorted, the difference signal "freezes" at some value near zero.

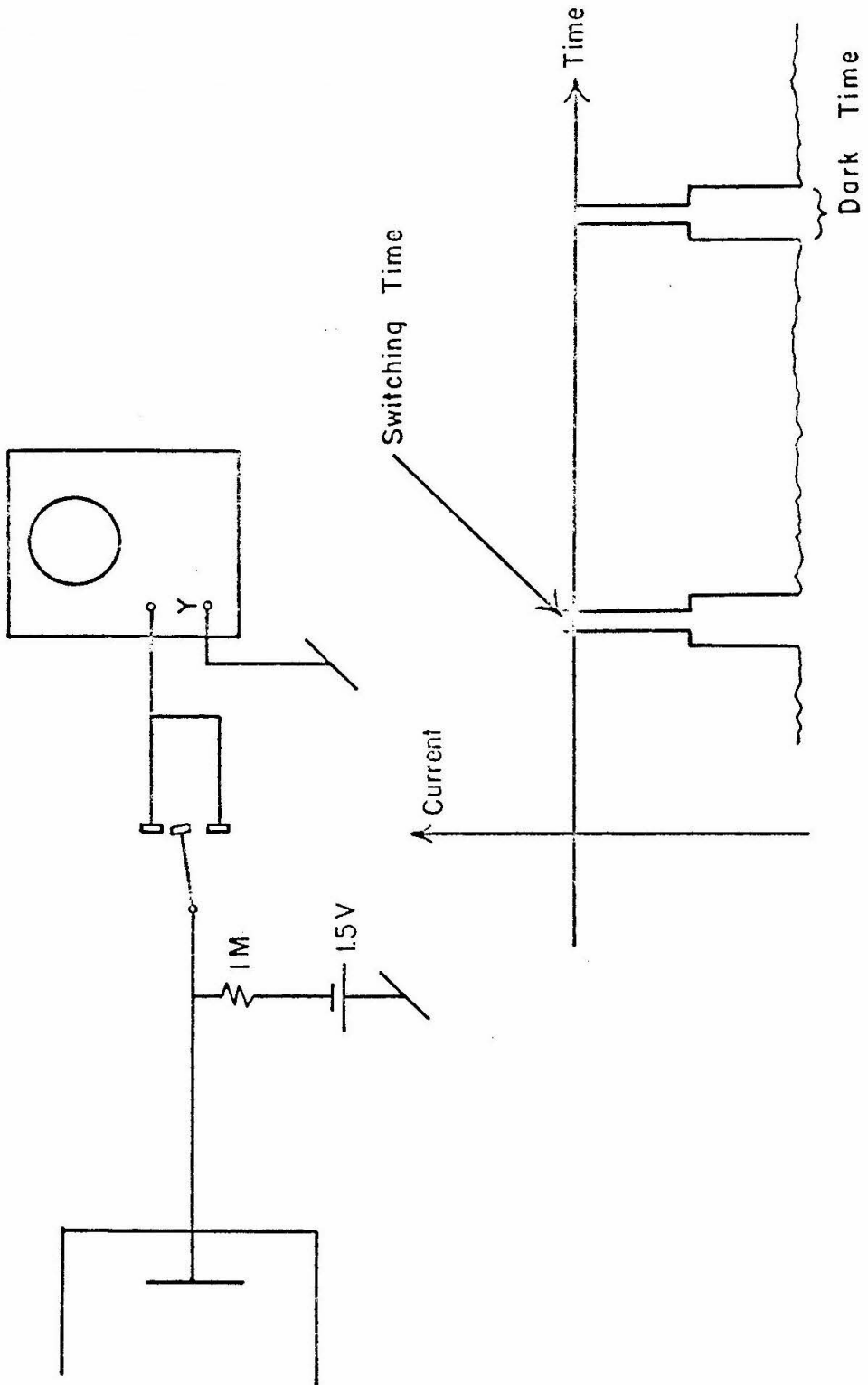


FIG. 6 SWITCHING WAVEFORM , CHECK

### E. Operational Amplifiers

Figure 7 is the schematic diagram of the operational amplifiers used in filtering, smoothing, subtracting, and recording the two current channels. They are two conventional chopper amplifiers sharing input and output SPDT choppers. The choppers are Steven-Arnold type 364 and were driven at 400 cycles per second by an oscillator. The high frequency response is dominated by the 1 M, 1 mfd time constant in the grid circuit of the output cathode follower. This allows non-oscillating operation with the output connected to the input. The potentiometer and battery in this same grid allow some offset adjustment. The open loop gain is about 9,000. The output noise with unity feedback is less than 1/10 mv. The open loop input impedance is 2 M. During operation, a usual value of the feedback resistor was  $R=1\text{ M}$ , and the feedback capacitor  $C = 10\text{ mfd}$ .

This made the closed loop characteristics approximately:

input impedance : 400 ohms

output impedance: .2 ohms

The low output impedance eliminates any loading effect of the chart recorder.

Checks were made on cross-talk between the amplifiers and on linearity, and it was determined that no systematic errors would be introduced by the amplifiers.

The feedback resistors and capacitors are selectable with a switch. Capacitors available are .1, 1, and 10 mfd. Values of resistance are .1M, 1M, 2M, 5M, 10M, and 100M.

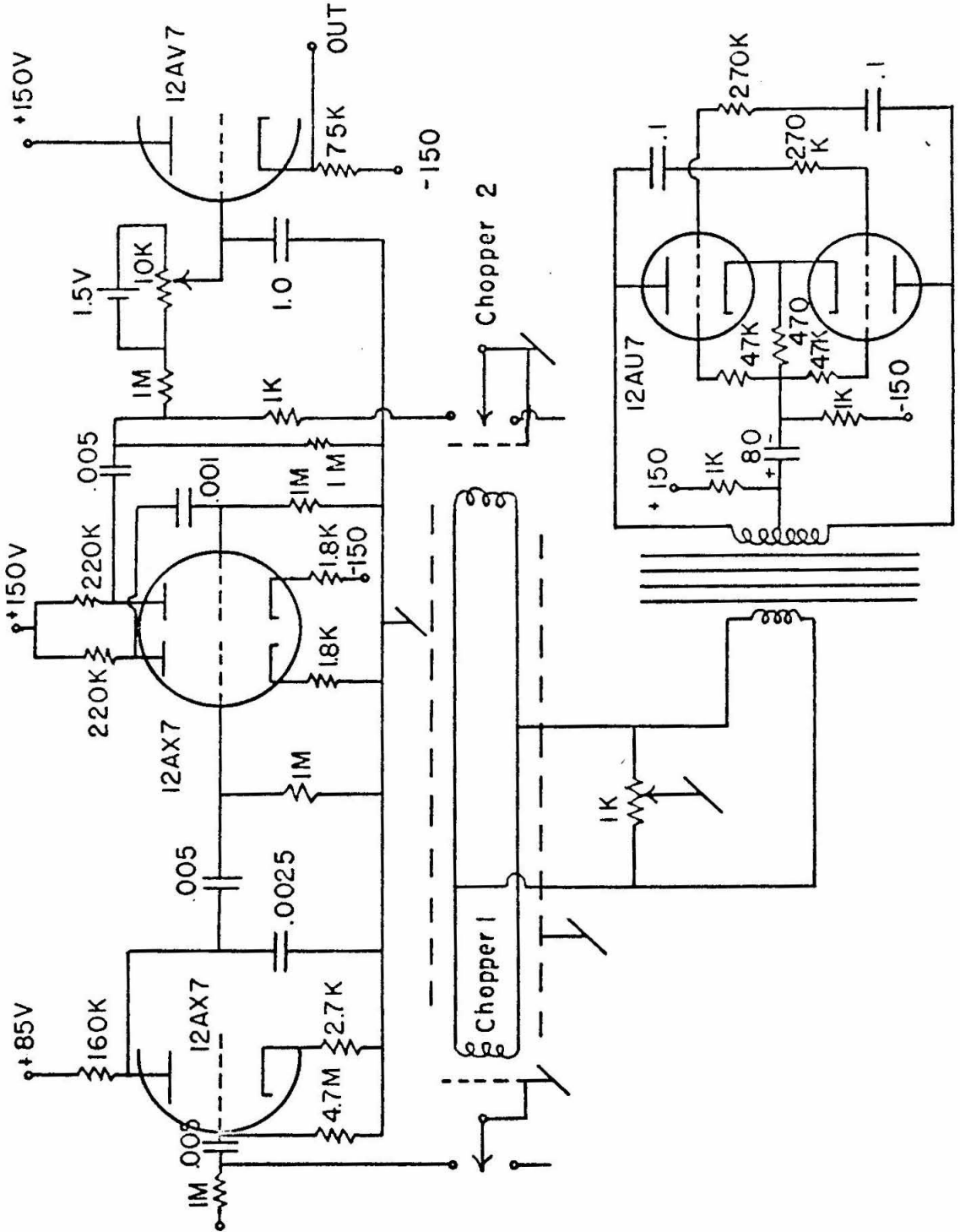


FIG. 7 CHOPPER AMPLIFIER

## F. Microbalance

39

A simple, yet effective microbalance was constructed to record the changes in weight of the deposit pan. The present automatic balance developed through an attempt to improve the sensitivity of a Cahn model M-10 manual electrobalance. The Cahn corporation's model RG has similar characteristics to the balance described here.

The balance uses the null-balance principle in which the mass to be measured hangs from the end of a beam (lever arm) and the resulting torque is counter-balanced by the torque from a current carrying coil in a magnetic field. The current required to hold the beam in equilibrium is calibrated against mass. Since the mass measurements are always made with the coil in the same position, no errors in the measurement are caused by non-ideal geometry of the magnetic field. A photoelectric beam-position sensor and a servo amplifier were used to keep the current and mass in balance and thus to provide a continuous record of mass on a strip chart recorder.

The schematic in figure 1 and the photograph of figure 15 in appendix II indicate the construction of the balance. Figure 8 is a schematic of the transistorized servo amplifier.

The torque motor for the balance is essentially a D'Arsonval ammeter with the jewelled bearings replaced by torsion fibers. The magnet and coil were removed from a 0-1 ma panel meter and the jewelled bearings replaced by a wire torsion suspension consisting of 1 1/2 inches of .001 inch diameter tungsten wire extending from each side of the coil. The support wires were spring loaded with about 100 grams of tension. This torsion support carried the current to the torque coil and eliminated the frictional sticking that was experienced with the jewelled bearings. The lever arm was a drawn glass tube about 3 inches long and 1/16 inch in diameter. It was cemented to the torque

coil in a direction perpendicular to the suspension wires. The deposit pan, mass about 30 mg, was suspended about five inches below one end of the balance beam on either a quartz fiber or a thin aluminum wire. On the other end of the glass tube from the mass was a sliding counterweight for manual adjustment of balance.

A sensitive position sensor was made from two RCA 6694-A photoresistive cells. These cells have a light sensitive strip only 1/16 inch wide and so made excellent position sensors. The two photocells were mounted side by side with the sensitive strips .15 inches apart. This assembly was placed next to a flag .15 inches wide attached to the balance beam, and the flag and photocells were illuminated by a small prefocussed light bulb. Motions of the balance beam would thus cause a difference in illumination between the two cells and the difference in output was fed to the servo amplifier shown in figure 8. The servo amplifier was designed largely by Robert Ashenfelter.

The response of the balance beam rotation to current inputs is quite well described by a second order, linear differential equation. Without feedback the balance had a period of about eight seconds and a damping time of 20 seconds. With feedback, the period is .2 seconds and because of some velocity feedback in the amplifier, the closed loop system is essentially critically damped. The damping action is provided by  $C_1$ , the 2 mfd. capacitor in the output circuit of the amplifier. The balance amplifier output is smoothed with an RC filter fed through a range attenuator to the chart recorder. The balance amplifier has a linear balancing range of plus and minus 2.5 mg and manual zero shifting controls give a range of plus and minus 5 mg. At the beginning of a run the counterweight on the balance beam arm

was adjusted to zero the balance amplifier with the manual zero shifter set at minus 5 mg. This procedure provided the use of the complete 10 mg range of the manual zero shifter.

Some difficulty was experienced with pendulum oscillations of the deposit pan. Two methods of hanging the pan were used. One was to hang the pan on a .006 inch diameter aluminum wire. The top part of the wire was bent into a hook and hung over a stirrup firmly attached to the end of the balance beam. This had the advantage that if any disturbance (such as the atomic beam) tended to make the pan swing like a pendulum, the sliding action at the point of suspension provided frictional damping and stopped the oscillation. The disadvantage of this was that vibrations of the system could and did cause shifts in the position of the hook in the stirrup and thus changed the effective lever arm. As a result, jumps of about five micrograms would occasionally occur in the output. The solution of this problem was to cement the suspension fiber to the beam. A quartz fiber was sometimes used in this application. In this case, swinging of the pan was damped by placing a permanent magnet near the aluminum pan. For atomic beams of cobalt and nickel, the magnet could not be used and the necessary damping was obtained by using the uncemented suspension.

The balance was calibrated by hanging a one mg weight onto the pan suspension point and adjusting the calibration potentiometer until full scale deflection on the 1000 microgram scale of the chart recorder was obtained. The weights used were Ainsworth balance riders. The manufacturer states a 5 microgram tolerance in the mass, and indeed the calibration was found to be constant within 1/2%. Further specifications are: 1/2 microgram noise, Scales: 1000, 500, 250, 100, 50, and 25 micrograms, servo gain about 1600.



### G. Atomic Beam Ionization Gauge.

Graphical differentiation of the microbalance recording to obtain the microbalance deposit rate is inherently noisy. Variations in the deposit rate of the atomic beam are always accompanied by corresponding changes in the impulse force that can obscure and confuse the nature of the change. In order to provide a continuous monitor of beam density, an ionization gauge was constructed and installed to provide an electrical signal proportional to the beam density. Figure 9 illustrates its location and structure in relation to the atomic beam. The cathode is a tungsten wire .002 inches in diameter by one centimeter long. Electrons are accelerated from this cathode through the grounded grid into the atomic beam area where they nominally have a kinetic energy equal to the cathode potential energy with respect to ground. Following the method of Boiko ( 16 ) the cathode voltage is operated between the ionization potential of the metal atoms in the beam and the ionization potential of the non-metallic atoms that constitute the residual gas in the vacuum system. Thus, ions produced can only be those of the metallic atom under study. The electron beam is collected by a plate on the other side of the atomic beam and the current is amplified and used to regulate the electron emission by changing the filament temperature. Generally, the collected current was operated at less than 15 microamps to minimize space charge effects.

The ions produced in the beam continue upward and are collected on a ring which is at a potential of minus thirty volts with respect to ground. The ion current is measured by an electrometer. Figure 10 is a schematic diagram of the electrometer used.

A small permanent magnet provided a magnetic field of about 500 gauss parallel to the electron travel. Several advantages were gained by the presence of this field. The field eliminated modulation of the electron beam by the sixty cycle magnetic field produced by the nearby furnace current. It would be expected that the field would constrain the electrons to a smaller region than if there was no field. But most important was the fact that if the field was removed the gauge became swamped with charged particles from the furnace. If the furnace was set at a negative potential of about ten volts with respect to ground, and the magnet was present, both the electron collector and the ion collector showed no current from the furnace. If the magnet was removed, several millamperes of current to the electron collector could be obtained from a hot furnace. Typical operation data were:

electron current  $10^{-6}$  amp

ion current  $10^{-9}$  amp

atomic beam current if totally ionized: about one amp

cathode voltage 8 volts

In operation the gauge produced an ion current that correlated well with deposit rate. A plot of ion current times the square root of temperature versus deposit rate was made. There was less than 2% departure from linearity over a factor of fifty in deposit rate. The linearity of the plot was taken as an indication that the mean velocity in the beam is indeed proportional to  $\sqrt{T}$  for a wide range of deposit rates.

The gauge had some serious limitations. The output had to be calibrated against the balance tracing and thus was not much more useful than the balance tracings themselves for obtaining the absolute  $f$ -values. It was found that the ion collection efficiency decreased a few percent upon

closing the shutter. This meant that it was not practical to regulate the beam density by varying the furnace temperature in response to changes in the ion current.

Because it would not work properly without the magnetic field, the gauge could not be used with ferromagnetic cobalt and nickel beams.

The gauge, however, did illuminate some of the problems in the beam formation process. In the case of silver, small globules of liquid metal were observed to condense in the orifice of the crucible from time to time. The ion current and the deposit rate at such times would change their ratio five to ten percent from that obtained with a clear orifice. In such cases, the equivalent width correlated better with the ion current than with the deposit rate. The gauge thus aided in interpretation of the data in cases where the apparent deposit rate changed.

The gauge was also useful as an indicator to aid in changing the beam density by a desired amount.

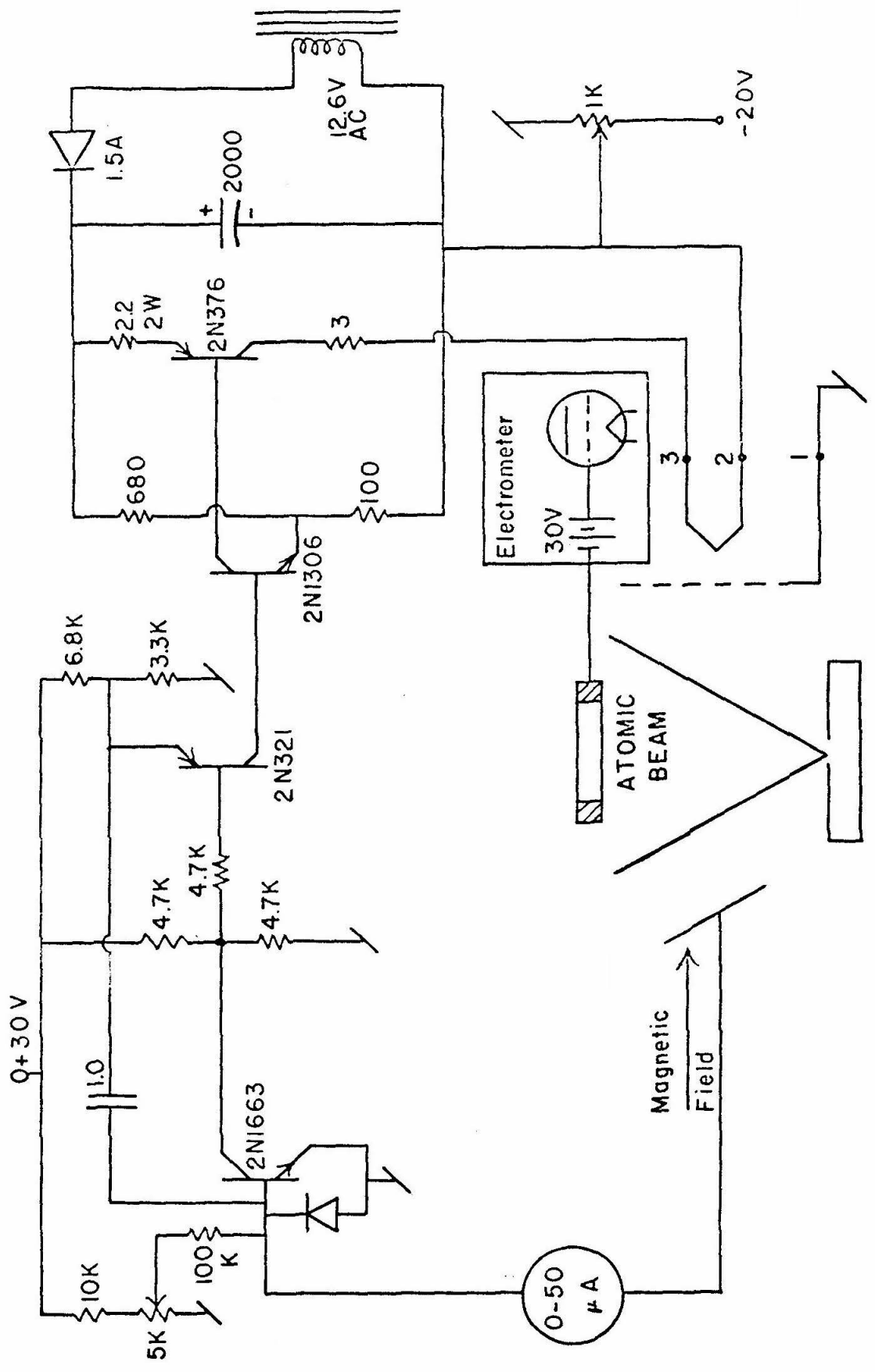


FIG. 9 IONIZATION GAUGE AND REGULATOR

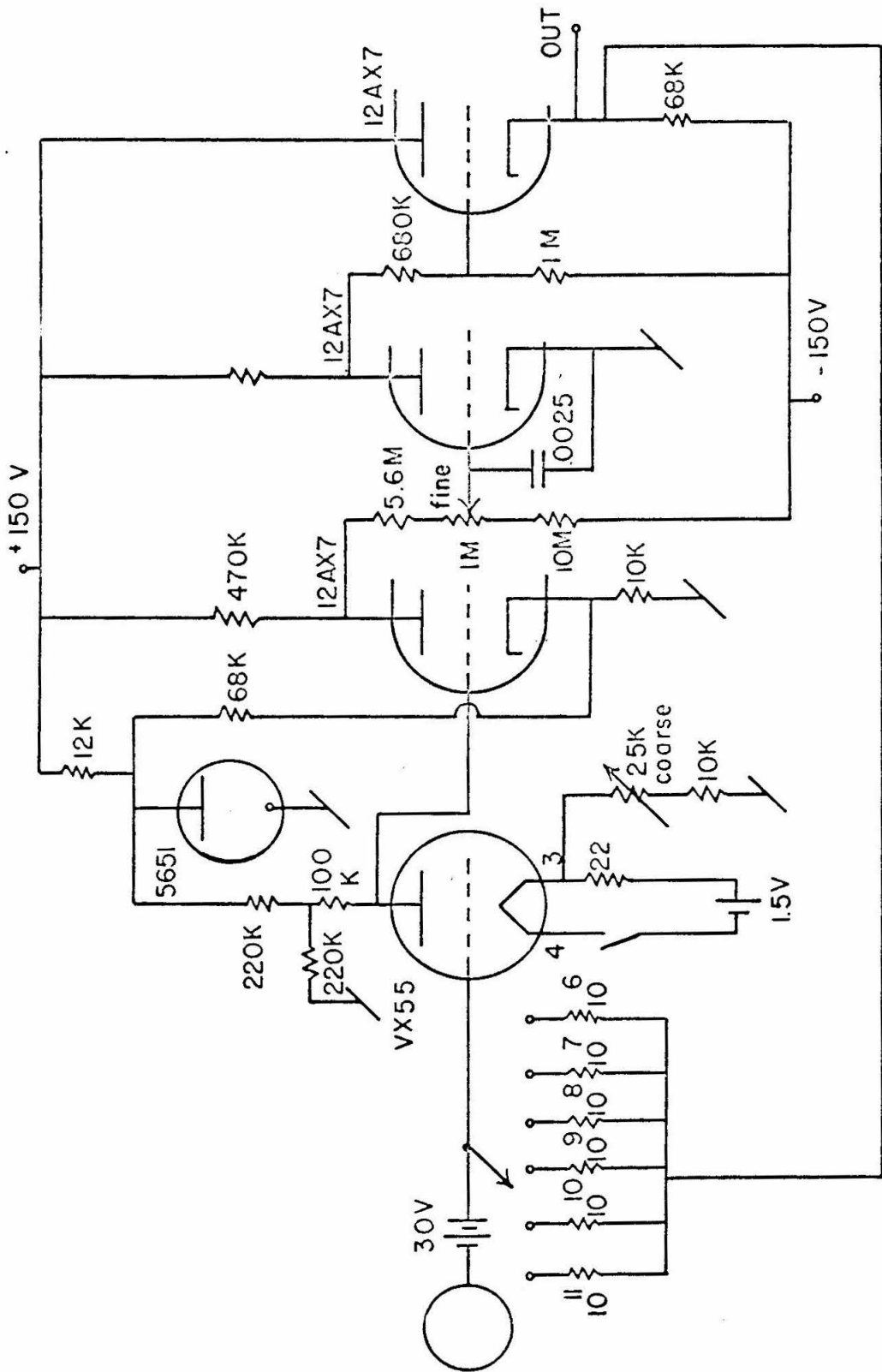


FIG. 10 ELECTROMETER USED WITH ION GAUGE

## H. Vacuum, Furnace, Temperature

The vacuum was obtained with a four inch oil diffusion pump with a water cooled baffle and a liquid nitrogen cold trap between it and the furnace chamber. Demountable joints were sealed with Viton O-rings. Sixteen hours of pumping were usually necessary to obtain a working pressure of  $2 \times 10^{-6}$  Torr as measured by a Veeco RG 75 K Bayard-Alpert gauge.

The electric furnace is described in detail by Davis (3). Internal parts exposed to strong radiation from the furnace are water cooled.

Temperatures of the interior of the crucibles were measured with an optical pyrometer. The temperature measuring system was checked at temperatures below  $1500^{\circ}\text{K}$  with a thermocouple in the interior of a crucible and found to be accurate within  $10^{\circ}$ . The estimated uncertainty in most temperature readings is  $\pm 15^{\circ}$ .

## V RESULTS AND COMPARISON WITH OTHER MEASUREMENTS

In the following pages, a discussion is given of other methods which have been used to produce  $f$ -values for the lines of this investigation. First the measurements of relative  $f$ -values are discussed and then the absolute  $f$ -value measurements.

Values of representative data are listed in tabular form, and a discussion of the problems and methods specific to each element is made.

The procedure in producing data was as follows: The furnace variac was set at a convenient position to obtain an atomic beam. The absorption line obtained was scanned a few times at this setting and microbalance recordings were made simultaneously for each line. The data tables contain the average temperature  $T$  during these scans, the range of values of  $W_e$  measured, the range of values of deposit rate  $G$ , the number of scans at the temperature  $T$ , and the average  $f$ -value. The average of all the values of  $f$  is given as the experimental value of  $f$ . In addition, representative Boltzman factors are listed in the data tables.

For gold and silver, the resonance doublets were studied. For cobalt and nickel, measurements were made on several of the strongest transitions from the low lying energy states.

### A. Relative f-Values.

King and co-workers have determined relative f-values for 256 lines of cobalt ( 17) and 134 lines of nickel ( 18 ) by the photographic measurement of equivalent widths of absorption lines formed by atoms in a graphite tube electric furnace. One of the important uses of the atomic beam absolute f-value measurements is to determine the absolute scale for these relative values. Aller, et al. ( 19 ) , for example, has stated a solar abundance for Co and Ni in terms of the reduction factor to King's relative values. Unfortunately the absolute f-values measured in this investigation ( the strongest absorption lines ) were not the most precisely determined of King's relative measurements.

For cobalt, the reduction factor was obtained by a comparison with the relative f-values measured by Ostrovsky and Penkin ( 20 ) with the hook method. Perhaps the most accurate measurements of relative f-values have been done in the Soviet Union using the method of anomalous dispersion or hook method. In this method, a column of absorbing atoms are placed in one path of a two beam interferometer. The interference fringe pattern is photographed at the focal curve of a stigmatic spectrograph. The phase shift caused by the anomalous dispersion in the wings of an absorption line causes a variation in the interference pattern that can be measured to give values of  $NfL$  from known parameters of the interferometer. A detailed description of this method is given by Prokofjew ( 20 ) and is available in English translation.

Islamov and Filippov ( 22 ) have measured relative f-values for the resonance doublet of silver using the hook method. They report a value of the ratio  $f_{3281}/f_{3384}$  of  $2.03 \pm .06$ . This value is listed in table III and labeled f (hook).

Ostrovskii and Penkin have measured relative f-values for strong absorption lines of cobalt ( 20 ). They estimate an accuracy of 5% for the lines that were measured in this investigation. These values are labeled f (hook) in tables VI and VIII. These cobalt relative values are published on the same relative scale as the more numerous total absorption measurements of King, et al. ( 17 ).

If L-S coupling is assumed to hold, the relative f-values for lines within a multiplet may be simply calculated. For the case of silver and gold, the squares of the ( dipole ) matrix elements between the common lower state and the two upper states will be in the ratio of the statistical weights of the upper states. From the well-known relations between f-values and dipole matrix elements, it can be shown that the ratio of the f-values is given by:

$$\frac{f_1}{f_2} = \frac{\lambda_2 g_1}{\lambda_1 g_2}$$

This quantity is listed in table III for the silver and gold resonance lines.

## B. Absolute f-values

Corliss and Bozman ( 23 ) of the National Bureau of Standards have recently published absolute gf-values obtained from intensities of 25,000 emission lines in a copper arc. This very important monograph contains gf-values for all lines which have been measured with the present atomic beam experiment. The values labeled f (NBS) in tables III, VI, and XI are the listed gf values divided by the statistical weight of the lower state. The authors state that the standard deviation for the individual log gf values is .27. This corresponds to a factor of error of 1.85.

The NBS gf-values were obtained from photographs of the emission spectra of elements added in small amounts to the electrodes of a copper arc. The intensities of the lines were estimated by eye relative to copper lines. The relative intensities of the copper lines were measured photoelectrically. The temperature of the arc was assigned an effective (Boltzman) temperature by studying the population of energy levels with the aid of 31 sets of relative f-values measured by other investigators. Then, relative f-values obtained from the temperature and the line intensities were put on an absolute scale by calibration with 37 published absolute f-values measured by others. The rather large error indicates the difficulty in determining the populations of the upper states.

The comparison of the NBS f-values with those of the present experiment shows agreement within the given experimental errors.

Hinnov and Kohn (24) conducted an investigation of collision broadening of lines emitted when metallic salts were introduced into an acetylene-air flame. Information concerning 3 of the absolute  $f$ -values of this experiment were obtained as a by-product. Measurements were made of both the intensity of emitted light and the absorption from a light beam passing through the flame as a function of the concentration of salt solution sprayed into the flame. These intensity-density data were used to give a curve of growth and hence measured values of  $NfL$  versus concentration. The ratio of  $NfL$  to the salt concentration was assumed to be the same for all metals that were completely dissociated in the flame. Using a sodium  $f$ -value,  $NfL$  was calibrated against the concentration of the salt solution. If the degree of dissociation of the salt in the flame was 100% absolute  $f$ -values were obtained, or if it seemed likely that the salt was only partially dissociated, lower limits were given for the  $f$ -values. Existing  $f$ -values were used to determine the degree of dissociation. The values given by this method seem to be accurate within 10-30 %, though the chemical behaviour of specific elements in the flame may lead to more uncertainties and limitations.

The  $f$ -values and limiting values marked  $f$  (flame) in tables III, VIII, and XI give the values reported by Hinnov and Kohn.

Estabrook (25) measured absolute  $f$ -values for three lines of nickel by measuring the total absorption of the lines absorbed from a continuous spectrum by nickel vapor heated in a closed tube at known temperature. The density of absorbing atoms was determined from vapor pressure data. King (26) revised the  $f$ -values on the basis of newer vapor pressure measurements by Morris, et al. (27). The revised values are listed in table XI and are used to make a fit to King's relative values. Although the revision by King (26) raised Estabrook's values by a factor of 1.6, the revised values are still a factor of 3.2 lower than the results of the atomic beam method.

• N. L. Moise has recently measured  $f$ -values for the Ag resonance lines by measuring the total absorption of a sample in a quartz absorption cell and obtaining  $N$  from vapor-pressure data published by the University of California Metallurgy group (29). His values of .45 and .175 for the silver resonance lines are listed by  $f$  (vapor press. ) in table III. The equivalent widths for Moise's determination of the  $f$ -values were measured in the same manner and with the same equipment as the atomic beam determination. The exact agreement of the  $\lambda 3281$   $f$ -values is fortuitous as the disagreement between .175 for  $f$  (vapor pressure ) and .22  $f$  (atomic beam) for  $\lambda 3383$  has not yet been understood.

Allen and Asaad ( 30 ) determined absolute f-values for the iron group elements and others from arc spectra of diluted copper alloys in a manner basically similar to the NBS method of Corliss and Bozman ( 23 ). The line intensities were measured photo-electrically, and the temperature calibration of the arc was made largely by the use of relative f-values measured in the laboratory of R. B. King.

In 1960 ( 31 ), Allen published a re-calibration of the previous data obtained by a comparison with available experimental values and theoretical values. The ratio, as given by Allen, of Allen's absolute scale to the relative scale of King and co-workers for Co and Ni (17, 18 ) is listed under "Reduction Factors" in tables VIII and XI. Allen lists a factor of error of  $10^{.2} = 1.5$ . Allen's value for the Ag resonance line  $\lambda$  3384 is listed in table III.

### C. Gold and Silver

Silver and gold were melted and vaporized in graphite crucibles heated in graphite furnace tubes. John Link ( 9 ) has described the method of manufacturing the furnace tubes and crucibles. The molten metals did not wet the graphite and the crucibles held enough metal to allow operation for a period of forty hours or more without refilling. The diameter of the crucible orifices was one mm.

During runs with silver and gold, the relative density of the atomic beam was monitored with the ionization gauge discussed in section IV H. Primarily, the gauge furnished qualitative information that pointed out sources of noise in the beam density measurements.

Attempts to make measurements on the Au line  $\lambda$  2428 produced only a lower limit of .15 for the f-value because of the low intensity of the light source at that wavelength. The photocurrent available at this wavelength was only 2.5 nanamperes compared with about 1000 nanoamperes on the long wavelength side of the Hg line  $\lambda$  2536. Investigations of the spectral composition of the light with Corning glass filters seemed to indicate that at least 2/3 of the light was scattered light from the spectral range of 2000-2800  $\text{A}^\circ$  passed by the filter used to separate orders.

Terrestrial gold consists of 100%  $\text{Au}^{197}$  with a nuclear spin of 3/2. The nuclear magnetic moment interaction splits the line  $\lambda$  2628 into 4 components. These components are listed below in tabular form.

| Relative Intensity | Separation from Center of Gravity of Line |
|--------------------|---|
| 5                  | 5.5                                       |
| 5                  | 6.1 ( $\text{mA}^\circ$ )                 |
| 5                  | - 9.8                                     |
| 1                  | - 9.1                                     |



The Doppler width,  $\Delta \lambda'_D$ , for Au was typically  $2.5 \text{ mÅ}^0$ . The line is split into separated components with ratios 5:3. Each such component, however, is somewhat wider than the width of a single Doppler component and would be expected to saturate less quickly than the single components. We would thus expect the actual curve of growth to lie between a curve constructed by splitting C into 4 parts with ratios 5:5:5:1, and a curve constructed by splitting C into two parts with ratios 3:5. Figure 4 indicates the nature of 4 different curves of growth obtained by the splitting of C various ways. The points are the experimental values of  $W_e/\Delta \lambda'_D$  and  $G/QT = C/f$  that were used to obtain the average value of .125 for the f-value of  $\lambda 2628$ . The horizontal position of the curves is consistent with  $f = .12$ . The f-values were calculated using the method that gives curve 3 in figure 4, that is, splitting C 3:5. At  $\frac{W_e}{\Delta \lambda'_D} = .500$ , the 4 part splitting curve and the 3:5 split give values of C that differ by 3%. It is estimated that the method of splitting used will contribute less than 2% error to the final value of f. The points marked with filled circles were not used in the determination of f.

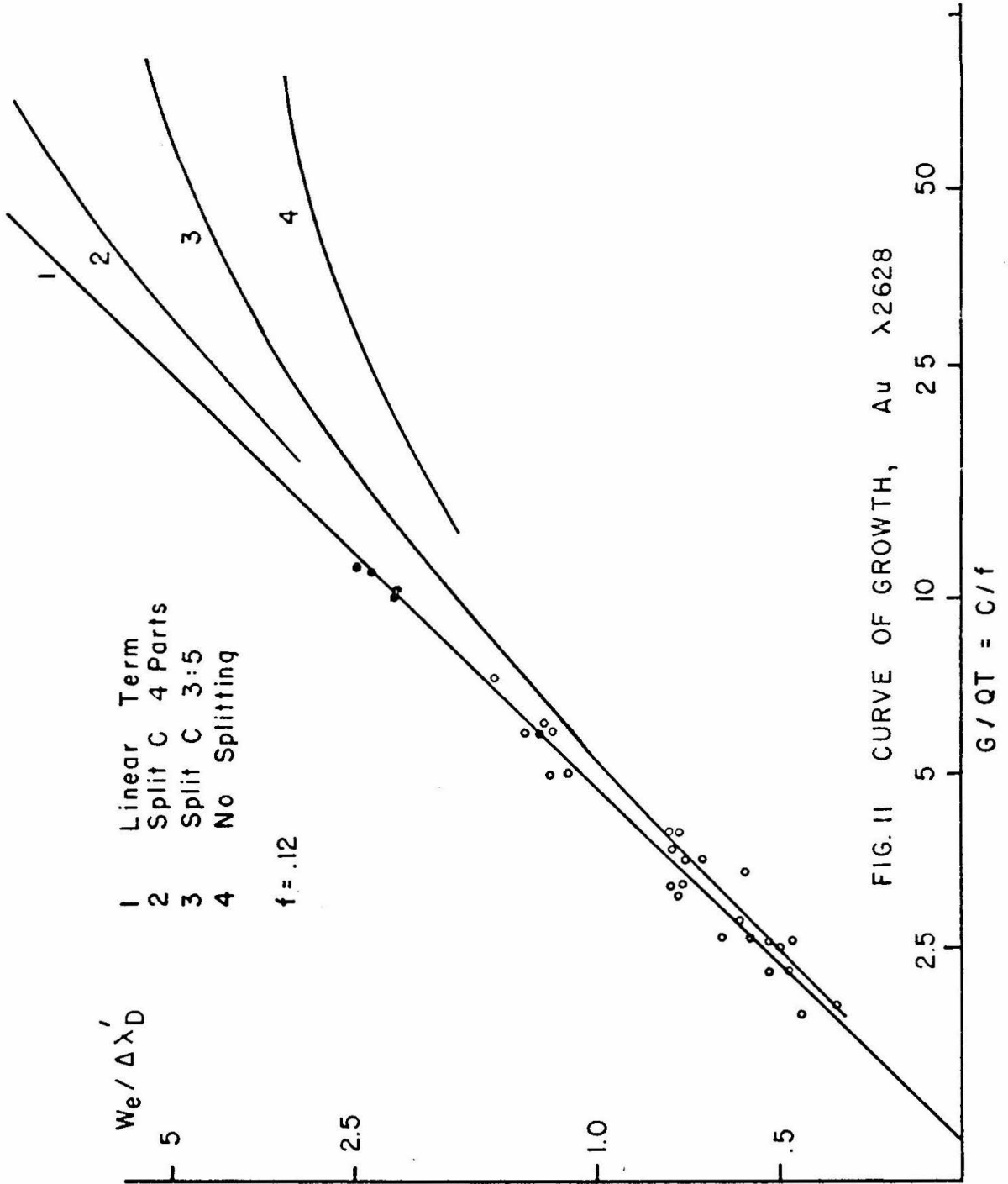


FIG. II CURVE OF GROWTH, Au  $\lambda 2628$

The silver resonance lines both exhibit 6 blended hyperfine components, three each from the isotopes  $\text{Ag}^{107}$  (52%) and  $\text{Ag}^{109}$  (48%). The maximum separation of these components is approximately  $7 \text{ mÅ}^0$  for lines. The Doppler width  $\Delta \lambda'_D$  was  $3.7\text{-}3.9 \text{ mÅ}^0$ . Roughly, these highly blended Doppler components should behave approximately twice as wide as a single component. In the analysis of the data, a curve of growth formed by splitting C into two equal parts was used. This is equivalent to assuming a Doppler width twice as large as  $\Delta \lambda'_D$ . Again, small equivalent widths were measured so as to minimize the uncertainties caused by the inexact curve of growth.

TABLE II  
Ag DATA

| T°K  | Range<br>We<br>mA° | Range<br>G<br>ng /sec. | No.<br>scans            | $\overline{f}$ | $\overline{\Delta}$ | f    |
|------|--------------------|------------------------|-------------------------|----------------|---------------------|------|
|      | $\lambda$ 3383     |                        | $^2S_{1/2} - ^2P_{1/2}$ |                |                     |      |
| 1357 | .65 - .89          | 35 - 36                | 5                       | .216           | .02                 | .215 |
| 1407 | 1.3 - 1.9          | 68 - 78                | 6                       | .212           | .01                 |      |
| 1446 | 2.3 - 2.9          | 120 - 135              | 6                       | .218           | .01                 |      |
|      | $\lambda$ 3280.68  |                        | $^2S_{1/2} - ^2P_{3/2}$ |                |                     |      |
| 1362 | 1.5 - 1.8          | 32 - 44                | 8                       | .453           | .03                 |      |
| 1350 | 1.1 - 1.3          | 26 - 28                | 6                       | .450           | .02                 | .45  |
| 1408 | 2.6 - 3.0          | 70 - 85                | 6                       | .443           | .02                 |      |

$$Z_0 = 1.7 \text{ inches}$$

$$\rho = .288 \text{ inches}$$

$$b = 2.76 \text{ inches}$$

$$Q = 4.62 \times 10^{-5}$$

$$\Delta\lambda'_D \sim 3.7 \text{ mA}^\circ$$

TABLE III

## Ag AND Au SUMMARY OF f- VALUES

| Element                                 | Ag                    |                | Au             |                |
|---|-----------------------|----------------|----------------|----------------|
|   | $\lambda 3384$        | $\lambda 3281$ | $\lambda 2676$ | $\lambda 2428$ |
| Upper state                             | $^2P_{1/2}$           | $^2P_{3/2}$    | $^2P_{1/2}$    | $^2P_{3/2}$    |
|   | Absolute f            |                |                |                |
| Atomic beam                             | .215                  | .45            | .125           | .15*           |
| Moise (25)<br>f-(Vapor Press)           | .175                  | .45            |                |                |
| f (flame)<br>(23)                       | .22                   | .39            |                |                |
| f (NBS)<br>(22)                         | .12                   | .27            | .06            | .08            |
| f (Allen)<br>(27)                       | .14                   |                |                |                |
|   | Relative f            |                |                |                |
| Atomic beam                             | 2.1                   |                |                |                |
| $\frac{2 \lambda_{1/2}}{\lambda_{3/2}}$ | 2.06                  |                |                | 2.20           |
| f (hook) (21)                           | 2.03 <sup>±</sup> .06 |                |                |                |

\*Undetermined scattered light.

#### D. Cobalt and Nickel

The crucibles that were used to form the cobalt beam consisted of a stabilized zirconia tube, closed at one end and plugged at the other. The orifice was formed in the side of the tube by grinding in such a way as to form a thin-edged hole. John Link (9) has described details of the usage and production of these crucibles. One important point in the use of these crucibles was that they had to be brought up to operating temperature gradually over the course of 30 minutes to prevent breakage caused by thermal shock.

Since nickel and cobalt are ferro-magnetic, the microbalance damping magnet and the atomic beam ionization gauge magnet had to be removed to prevent errors in the weighing of the deposited metal. ( See section IV, G )

The small f-values and complex, low-lying, term structure of nickel and cobalt required higher beam densities than silver and gold by a factor of approximately 10. The orifice in the crucible was enlarged to 3 mm diameter in order to increase the ratio of the mean free path in the furnace to the diameter of the orifice.

$\text{Co}^{59}$  has a nuclear spin of  $7/2$  and constitutes essentially 100% of natural cobalt samples. The hyperfine structure due to nuclear magnetic moment interaction with the electrons is relatively complex. For example, the ground state transition  $\lambda 3524.9$  ( $a^4F_{9/2} - z^4F_{9/2}$ ) should exhibit 22 hyperfine components. The ground term exhibits a maximum splitting of  $61 \text{ m}\text{\AA}^0$ . In view of this large splitting, measurements were made with values of  $W_e/\Delta\lambda'_D$  less than .3, and values of C were taken as given by equation 6, the linear approximation. The Doppler width  $\Delta\lambda'_D$  was in the order of  $6 \text{ m}\text{\AA}^0$ . The uncertainty introduced by this approximation is estimated to be less than 1%, certainly small compared with the uncertainty in the beam density determination.

A comparison of the atomic beam f-values of cobalt with the relative f-values of King, et al. (17) and of Ostrovskii and Penkin (20) provided evidence that the excited levels of cobalt are less densely populated than is expected for a Boltzman distribution at the temperature of the furnace. Roughly speaking, the .1-.4 ev energy levels were found to be under-populated as if the temperatures used in calculating Boltzman factors were too high. Initially, f-values were calculated from the raw data using Boltzman factors calculated at the working temperatures of the furnace - 2100-2250°K. These data are listed in tables IV-VI. Figure 12 compares the atomic beam f-values with the two sets of relative values as a function of the lower energy level of the transition. The ordinate (log scale) is the ratio of f (atomic beam) to f(relative). The abscissa is the energy of the lower state of the transition in electron volts. The error flags include the 5-10% relative error in the atomic beam determination and 15 and 10%, respectively, for the relative errors in the values of f(absorption tube by King) and f(hook). It is seen that the ratios do not lie on a horizontal line but show a systematic decrease with energy of the lower state. This can be interpreted as a depopulation of the lower energy states in comparison with the energy distribution expected at the furnace temperature. Attempts to eliminate the effect have been unsuccessful. The question then arises: Can corrections for the depopulation be made in order to obtain accurate absolute f-values? Also, what is the mechanism that causes the effect?

Values of equivalent width obtained in the experiment lead to optically measured values of  $N_i f_{i \text{ true}}$ , where  $N_i$  is the density of atoms in the  $i^{\text{th}}$  lower state and  $f_{i \text{ true}}$  is the true f-value for a transition from the  $i^{\text{th}}$  lower state. If the  $f_{i \text{ true}}$ 's are known on a relative scale, the experimental

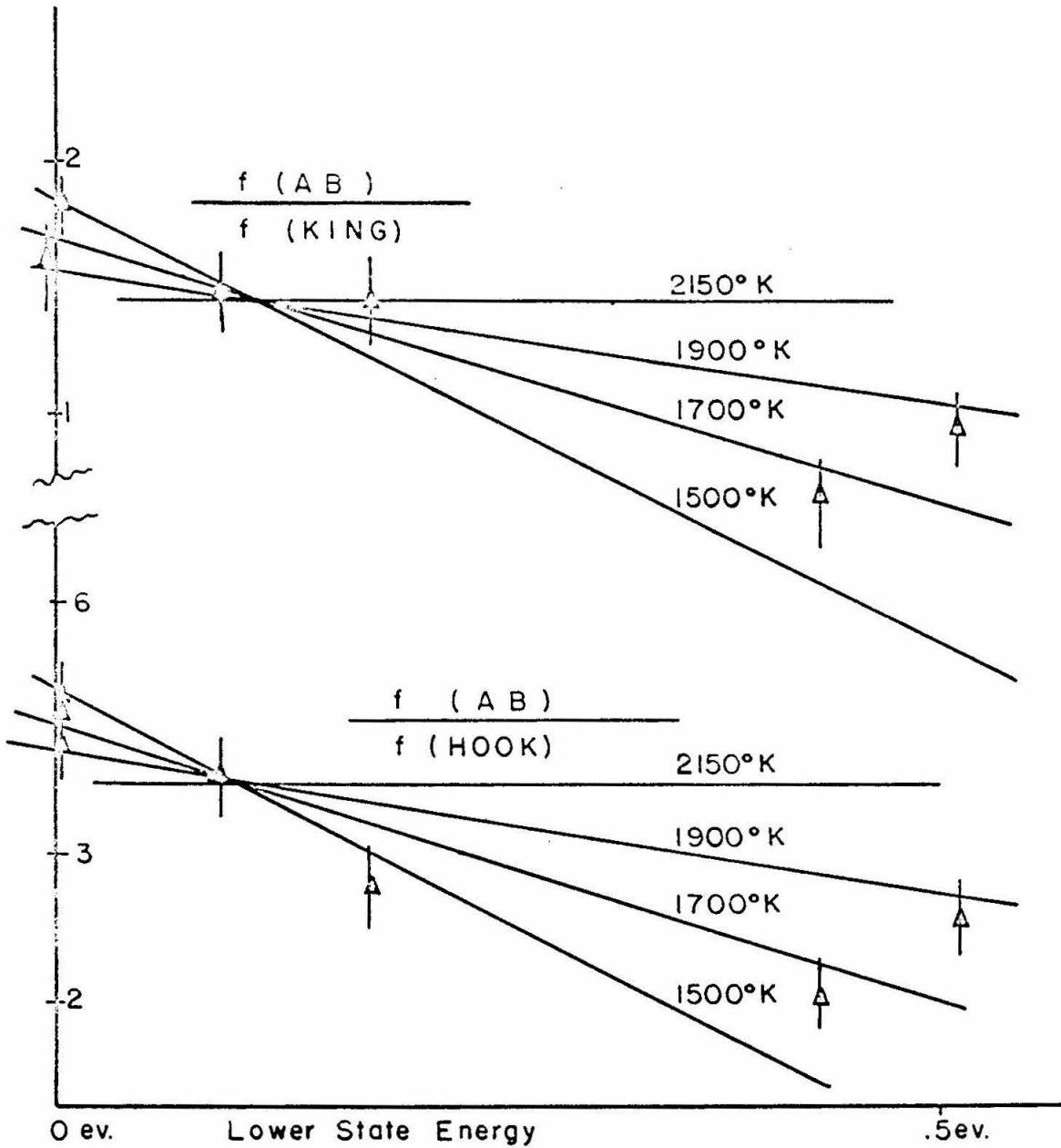


FIG.12 COBALT DEPOPULATION

data can be used to yield empirical relative values for the  $N_i$ 's.

At the temperatures of the furnace,  $T_f$ , around 2150°K, f-values,  $f_i$ , were calculated by dividing the optical value of  $N_i f_i$  true by  $N (B.f.)_{if}$ , where  $(B.f.)_{if}$  is the Boltzman factor appropriate to the furnace temperature  $T_f$  and for the  $i^{\text{th}}$  energy level. If the internal energy distribution of the atoms in the beam were actually described by a Boltzman distribution at some other temperature  $T_b$ , then we obtain as a correction formula:

$$f_i \text{ true} = \frac{(B.f.)_{if} f_{if}}{(B.f.)_{ib}} = \frac{U(T_b)}{U(T_f)} e^{-\frac{E_i}{K} \left( \frac{1}{T_f} - \frac{1}{T_b} \right)}$$

where  $(B.f.)_{ib}$  is the Boltzman factor appropriate to the temperature  $T_b$  and  $U(T)$  is the partition function,

$$U(T) = \sum_i g_i e^{-\frac{E_i}{KT}}$$

Thus, on a semilog plot, the ratios of calculated f-values at the furnace temperature  $T_f$  to the true (relative) f-values would form a straight line as a function of the lower energy values,  $E_i$ . The slope would be proportional to  $1/T_f - 1/T_b$ . The slopes of the lines drawn in figure 12 correspond to temperatures of 1500, 1700, and 1900°K if  $T_f$  is taken to be 2150°K. From a consideration of figure 12, it seems that the energy level population as obtained empirically can be described, within the scatter, by an effective distribution temperature of  $1700 \pm 200$ °K. Some of the uncertainty and ambiguity in describing the distribution by an effective beam temperature  $T_b$  is due to the fact that  $T_f$  varied over a range of temperatures rather than having a unique value. However, no significant change in the initial f-values as a function of furnace temperature was observed. A further difficulty lies in the lack of accuracy in the relative f-values. For example, a similar comparison with the NBS

f-values (23) yields an effective temperature of  $1950^{\circ}\text{K}$ .

If the f-values are corrected on the basis of an effective temperature of  $1700 \pm 200^{\circ}\text{K}$ , what is the change in the f-values? Table VII lists the Boltzman factors for the eight lowest states of cobalt at three different temperatures. The last column lists the factor (with its error) by which  $f_f$  must be multiplied to make the correction to  $1700 \pm 200^{\circ}\text{K}$  from  $2150^{\circ}\text{K}$ . It can be seen that the correction is less ambiguous for the low energy states than for the high energy states.

It was felt that the corrected f-values for the four ground state transitions would provide the most reliable data for the purpose of reducing the relative scale to absolute values. Table VIII lists the corrected f-values for these transitions and the reduction factors necessary to reduce the relative values of f(hook) (19) and f(King) (16) to an absolute scale. The reduction factor determined by Allen (28) is also listed.

In effect, the measurements of f-values for transitions arising from the higher states have been used to determine the distribution of atoms among the energy levels under the experimental conditions. This empirical distribution was then used to calculate the f-values for the ground state transitions. The one parameter theory (Boltzman distribution) for describing the energy distribution is not well established but, fortunately, the density of the ground state as determined by the theory is relatively insensitive to variations in the effective temperature.

The mechanism of the depopulation has yet to be determined. The most plausible explanation which has been suggested as a mechanism is the effect of collisions in the gas streaming out from the crucible orifice. Just inside the orifice and for some distance outside the orifice, the atoms suffer collisions with other atoms traveling in the same direction (outward). The

average relative velocity of collisions is thus less than for the conditions inside the crucible where atoms traveling in opposite directions collide. If this is the mechanism, it would be expected that the depopulation would disappear if the crucible could be operated at a lower internal pressure and therefore a longer mean free path. Attempts to verify this experimentally have been inconclusive. Measurements have been made with changes of a factor of 8 in beam density and no significant change in the atomic beam relative  $f$ -values has been observed. In order to extend the measurements to yet lower beam densities, the furnace could be enlarged or the light beam passed through the atomic beam more than one time.

TABLE IV  
 COBALT I DATA  $aF_{9/2}$  GROUND STATE

| $T^{\circ}K$ | Range<br>We<br>$mA^{\circ}$ | Range<br>G<br>$\mu g / sec$ | No.<br>scans | $\bar{f}$             | $\bar{\Delta}$ | f     |
|--------------|-----------------------------|-----------------------------|--------------|-----------------------|----------------|-------|
|              | $\lambda$ 3526.85           |                             |              | $a^4F - z^4F$         |                |       |
| 2175         | 3.2 - 3.7                   | 1.1 - 1.3                   | 5            | .0235                 | .001           |       |
| 2124         | 1.4 - 2                     | .58 - .73                   | 11           | .0220                 | .002           |       |
| 2215         | 2.2 - 3.2                   | .8 - 1.2                    | 3            | .0214                 | .001           |       |
| 2141         | 3.3 - 3.9                   | .52 - .61                   | 4            | .0221                 | .002           | .0232 |
| 2200         | 1.4 - 1.7                   | .47 - .55                   | 6            | .0259                 | .001           |       |
| 2250         | 3.0 - 3.7                   | .93 - 1.1                   | 2            | .0260                 | .0006          |       |
|              | $\lambda$ 3465.792          |                             |              | $a^4F - z^4G^{\circ}$ |                |       |
| 2141         | 3.1 - 3.4                   | .61 - .65                   | 4            | .0183                 | .0007          |       |
| 2090         | 1.4 - 2                     | .30 - .36                   | 8            | .0187                 | .0007          |       |
| 2186         | 1.9 - 2                     | .32 - .34                   | 1            | .0209                 | .0009          | .0197 |
| 2250         | 2.5 - 2.6                   | 1                           | 2            | .0203                 | .0008          |       |
| 2200         | 1.1 - 1.5                   | .50 - .54                   | 6            | .0215                 |                |       |
|              | $\lambda$ 3412.63           |                             |              | $a^4F - z^4D$         |                |       |
| 2200         | .8 - 1.4                    | .7 - 1.1                    | 10           | .0195                 | .001           |       |
| 2250         | 1                           | .5                          | 2            | .0176                 |                |       |
| 2045         | 1.0 - 1.1                   | .23 - .25                   | 4            | .0156                 |                |       |
| 2110         | 1.6 - 2.2                   | .39 - .47                   | 6            | .0150                 |                | .0166 |
| 2202         | 1.2 - 1.5                   | .26 - .30                   | 13           | .0174                 |                |       |
| 2270         | 1.2 - 2.0                   | .20 - .40                   | 5            | .0179                 | .001           |       |
| 2193         | 1.3 - 1.7                   | .29 - .34                   | 8            | .0164                 |                |       |
|              | $\lambda$ 3044.004          |                             |              | $a^4F - y^4F$         |                |       |
| 2110         | 2.1 - 2.3                   | .37 - .40                   | 4            | .0252                 | .0003          | .026  |
| 2038         | .8 - 1.0                    | .17 - .18                   | 8            | .0264                 | .005           |       |

B. f.  $\sim$  .49

TABLE V  
COBALT I *b* STATES

| $T^{\circ}K$ | Range<br>We<br>$m\text{\AA}^{\circ}$ | Range<br>G<br>$ng./sec$ | No.<br>scans | $\overline{f}$ | $\overline{\Delta}$ | $f$                 |
|--------------|--------------------------------------|-------------------------|--------------|----------------|---------------------|---------------------|
|              | $\lambda$ 3412.34                    |                         |              |                |                     |                     |
|              |                                      |                         |              |                |                     | $b^4F_{7/2} - y^2G$ |
| 2045         | .22 - .30                            | 10 - 11                 | 4            | .0808          | .01                 | .0838               |
| 2110         | .46 - .56                            | 19 - 22                 | 6            | .0858          | .01                 |                     |
|              | $\lambda$ 3405.120                   |                         |              |                |                     |                     |
|              |                                      |                         |              |                |                     | $b^4F_{9/2} - y^4F$ |
| 2090         | .85 - 1.1                            | 23 - 32                 | 6            | .132           | .01                 | .13                 |
|              | $\lambda$ 3453.514                   |                         |              |                |                     |                     |
|              |                                      |                         |              |                |                     | $b^4F_{9/2} - y^4G$ |
| 2090         | .6 - 1.2                             | 11 - 22                 | 6            | .204           | .01                 |                     |
| 2040         | .7 - .9                              | 14 - 15                 | 3            | .202           | .01                 | .169                |
| 2080         | .5 - 1.2                             | 16 - 26                 | 15           | .149           | .03                 |                     |

TABLE VI

SUMMARY OF COBALT RESULTS UNCORRECTED FOR  
DEPOPULATION OF (.1 - .5)ev. STATES

| E(ev.) | $\lambda$ | (17)<br>f(King) | (20)<br>f(Hook) | (23)<br>f(NBS) | f(AB) |
|--------|-----------|-----------------|-----------------|----------------|-------|
| 0      | 3526.8    | 2,300           | 983             | .048           | .023  |
| 0      | 3465.8    | 2,220           | 875             | .042           | .020  |
| 0      | 3412.6    | 1,120           | 710             | .02            | .017  |
| 0      | 3044.0    | 1,400           | 1,360           | .044           | .026  |
| .513   | 3412.3    | 6,560           | 7,000           | .24            | .084  |
| .432   | 3405.1    | 13,500          | 13,600          | .27            | .13   |
| .432   | 3453.5    | 21,700          | 14,700          | .46            | .17   |
| .101   | 3575      | 942             | 696             | .028           | .013  |
| .174   | 3529      | 997             | 1,030           | .027           | .014  |

TABLE VII  
 BOLTZMAN FACTORS AND DEPOPULATION  
 CORRECTION FACTORS FOR COBALT

| Lower level | E ev. | Boltzman Factors (per cent) |            |            | Correction factor          |
|-------------|-------|-----------------------------|------------|------------|----------------------------|
|             |       | T = 2100°K                  | f = 1800°K | T = 1500°K | $f_b/f_f$                  |
| aF 9/2      | 0     | 50.5                        | 55         | 60.6       | (.884)(1 <sup>±</sup> .07) |
| aF 7/2      | .101  | 23                          | 22.9       | 22         | (1.02)(1 <sup>±</sup> .02) |
| aF 5/2      | .174  | 11.5                        | 10.7       | 9.4        | (1.10)(1 <sup>±</sup> .05) |
| aF 3/2      | .224  | 5.9                         | 5.2        | 4.2        | (1.25)(1 <sup>±</sup> .15) |
| bF 9/2      | .432  | 4.7                         | 3.4        | 2.0        | (1.65)(1 <sup>±</sup> .45) |
| bF 7/2      | .513  | 2.4                         | 1.6        | .90        | (1.8)(1 <sup>±</sup> .50)  |
| bF 5/2      | .581  | 1.2                         | .78        | .39        | (1.92)(1 <sup>±</sup> .65) |
| bF 3/2      | .630  | .63                         | .38        | .18        | (2.17)(1 <sup>±</sup> .70) |

$f_f$  is f- value calculated for T = 2150°

$f_b$  is corrected f- value.

TABLE VIII

COBALT I GROUND STATE f- VALUES CORRECTED FOR  
MEASURED DEPOPULATION OF (.1-.5) ev STATES

| $\lambda$ | Weight | f(hook)<br>(20) | f(flame)<br>(24) | f(AB)(corrected) |
|-----------|--------|-----------------|------------------|------------------|
| 3526.8    | 3      | 983             | >.028            | .020             |
| 3465.8    | 2      | 875             |                  | .0175            |
| 3412.6    | 4      | 710             |                  | .0147            |
| 3044.0    | 1      | 1360            |                  | .023             |

#### Reduction Factors, Cobalt

King, et al. (17) and Ostrovskii, et al. (20) list their f values on the same relative scale. The fit is made to (20).

$$\frac{f(\text{AB}) \text{ corrected}}{f(\text{King})} = 2.0 \times 10^{-5} = 10^{-4.70}$$

$$\frac{f(\text{Allen})}{f(\text{King})} = 2.3 \times 10^{-5} = 10^{-4.65}$$

## Nickel

The difficulty of upper state depopulation that was seen in the cobalt measurements can certainly be expected to occur with nickel. The nickel data were measured at almost identical furnace temperatures, geometry, and beam fluxes as with cobalt. The chemical behaviour and mass of Ni and Co are similar. Unfortunately, no lines arising from the higher states of nickel have sufficiently large f-values for convenient measurement with the present atomic beam apparatus. Hence no empirical measure of the energy level populations in the beam is available. Five of the six transitions studied are from the  $^3D_3$  (.035ev) state. If the population of this state were to be corrected from a Boltzman temperature of 2150<sup>o</sup>K to an effective temperature of 1700<sup>o</sup>K as was done with cobalt, the  $^3D_3$  f-values would be multiplied by (.95 ± .03). Because this correction is smaller than in the corresponding case of cobalt, and because there is no direct evidence for the depopulation of the upper nickel levels, this 5% correction was not made.

TABLE IX  
 NICKEL I  $^3D_3$  TRANSITIONS

| $T^\circ K$        | Range<br>We<br>$mA^\circ$ | Range<br>G<br>$ng./sec$ | No.<br>scans | $\overline{f}$ | $\overline{\Delta}$ | f    |
|--------------------|---------------------------|-------------------------|--------------|----------------|---------------------|------|
| $\lambda 3524.54$  |                           |                         |              |                |                     |      |
| 2173               | 2.4 - 2.9                 | 78 - 98                 | 6            | .120           | .007                |      |
| 1983               | 1.6 - 1.8                 | 47 - 49                 | 6            | .116           |                     |      |
| 2036               | 2.6 - 2.8                 | 79 - 84                 | 6            | .113           |                     | .116 |
| 1959               | .7 - 1.1                  | 20 - 30                 | 4            | .112           | .007                |      |
| $\lambda 3461.62$  |                           |                         |              |                |                     |      |
| 2181               | 2.2 - 2.9                 | 190 - 230               | 4            | .0478          | .001                |      |
| 2103               | 1.7 - 3.4                 | 110 - 250               | 11           | .0541          | .003                |      |
| 2065               | .7 - 1.8                  | 51 - 140                | 9            | .0457          |                     | .051 |
| 2036               | 1.4 - 1.7                 | 98 - 110                | 6            | .0517          | .003                |      |
| 1978               | .76 - .87                 | 45 - 54                 | 7            | .0543          |                     |      |
| $\lambda 3414.77$  |                           |                         |              |                |                     |      |
| 2011               | 1.3 - 1.7                 | 43 - 54                 | 6            | .108           | .005                |      |
| 1980               | 1.1 - 1.5                 | 37 - 42                 | 6            | .126           | .01                 | .116 |
| 2036               | 2.2 - 2.6                 | 66 - 84                 | 7            | .115           | .005                |      |
| $\lambda 3392.93$  |                           |                         |              |                |                     |      |
| 2113               | .49 - 1.6                 | 50 - 160                | 11           | .0324          | .002                | .032 |
| $\lambda 3050.819$ |                           |                         |              |                |                     |      |
| 2098               | 2.2 - 2.9                 | 116 - 127               | 6            | .101           | .01                 | .096 |
| 2045               | 1.6 - 1.7                 | 76 - 81                 | 6            | .091           | .007                |      |

B. f.  $\sim .26$   
 $\Delta\lambda_D' \sim 5.8 mA^\circ$

TABLE X  
 NICKEL I  $^3F_4$  TRANSITION

| $T^{\circ}K$      | Range<br>We<br>mA $^{\circ}$ | Range<br>G<br>ng /sec | No.<br>scans | $\overline{f}$ | $\overline{\Delta}$ | f    |
|-------------------|------------------------------|-----------------------|--------------|----------------|---------------------|------|
| $\lambda$ 3369.57 |                              |                       |              |                |                     |      |
| 2070              | .78 - 1.1                    | 170 - 200             | 6            | .0193          | .002                |      |
| 2113              | .82 - .99                    | 150 - 180             | 6            | .0202          | .001                | .019 |
| 2091              | .60 - .79                    | 150 - 170             | 6            | .0174          | .002                |      |

Bf  $\sim$  .39

TABLE XI  
NICKEL I SUMMARY AND COMPARISON

| $J_1 - \text{Jup}$ | $\lambda$ | (24)<br>f(flame) | (18)<br>f(King) | (23)<br>f(NBS) | Estabrook | f(AB) |
|--------------------|-----------|------------------|-----------------|----------------|-----------|-------|
| 3 - 2              | 3524.5    | >.19             | 786             | .121           | .03       | .116  |
| 3 - 4              | 3461.6    |                  | 343             | .082           | .015      | .051  |
| 3 - 4              | 3414.8    |                  | 644             | .14            | .028      | .116  |
| 3 - 3              | 3392.99   |                  | 258             | .059           |           | .032  |
| 3 - 4              | 3050.8    |                  | 686             | .114           |           | .096  |
| 4 - 3              | 3369.6    |                  | 171             | .039           |           | .019  |

Reduction Factors, Nickel

$$\frac{f(AB)}{f(King)} = 1.43 \times 10^{-4} = 10^{-3.84}$$

$$\frac{(31)f(Allen)}{f(King)} = 2.1 \times 10^{-4} = 10^{-3.67}$$

$$\frac{f(Estabrook)}{f(King)} = .43 \times 10^{-4} = 10^{-4.37}$$

## E. Errors

We recall equation 2 connecting the f-value with the experimental data for small equivalent width.

$$W_e = \frac{\pi e^2}{m c^2} \cdot f \lambda_0^2 \frac{2}{v} G \left( \frac{b^2 + \rho^2}{\rho^2} \right) \frac{\sin \delta}{\bar{R}_0}$$

Following is a tabulation of the factors in this equation and their estimated errors. The random errors are average values for a single determination and the systematic error estimates are thought to be a safe upper limit.

| Quantity  | Random Error | Systematic Error |
|---|--------------|------------------|
| Curve of Growth   | 0%           | 2%               |
| Equivalent Width, $W_e$   | 15%          | 5%               |
| v, mean velocity of beam  | 2%           | 2%               |
| Boltzman Factors  |              |                  |
| G Sticking Coefficients   | 10%          | 5%*              |
| Deposit Rate  |              |                  |
| Beam Geometry   |              |                  |
| $\left( \frac{b^2 + \rho^2}{\rho^2} \right) \left( \frac{\sin \delta}{\bar{R}_0} \right)$ geometrical factors | .2%          | 1%               |
| <hr/>   |              |                  |
| f   | 18%          | <15%*            |

The values of error for f were obtained by calculating the square root of the sum of the squares of the random errors and by adding the systematic errors. For each f-value determined, enough data were taken to reduce the expected random error in the average to less than 5%.

---

\* Perhaps 5-8% larger for cobalt and nickel.

References

- ( 1) Kuhn, H. G. (1962), Atomic Spectra (1st ed.; New York: Academic Press) pp 59ff.
- ( 2) Wessel, G. (1949), Z. f. Physik, 126, 440.
- ( 3) Davis, M. H. (1955), Thesis (Calif. Inst. of Tech.).
- ( 4) Bell, G. D. (1957), Thesis (Calif. Inst. of Tech. ).
- ( 5) Bell, G. D., Davis, M.H., King, R.B., and Routly, P.M. (1956), Ap. J., 127, 775.
- ( 6) Bell, et al. (1959), Ap. J., 129, 775. ,
- ( 7) Bell, G.D., and King, R.B. (1961), Ap. J., 133, 718.
- ( 8) King, R. B., (1963), Proceedings of Symposium on Quantitative Spectroscopy and Applications in Space Science. Calif. Inst. of Tech. (to be published by Pergammon Press).
- ( 9) Link, J.K. (1963), Thesis (Calif. Inst. of Tech. ).
- (10) Unsöld, A. (1955), Physik der Sternatmosphären (2nd ed.; Berlin: Springer-Verlag), pp. 267-370.
- (11) Landolt-Bornstein (1952), Zahlenwerte u. Funktionen I Band, 5 Teil (Berlin : Springer-Verlag) pp 1-63.
- (12) Greiner, J.H., Yetter, L.R., and Gleason, F.R.,(1959), Proceedings, 6th National Symposium on Vacuum Technology (Pergammon Press) p. 222.
- (13) Wexler, S., (1958), Rev. Mod. Physics, 30, 402.
- (14) Strong, J., (ed.) (1938) Procedures in Experimental Physics, (New York, Prentice Hall).
- (15) Stahl, A.H., (1959), J. Opt. Soc. Am. 49, 381.
- (16) Boiko, B. A., (1961), Instruments and Experimental Techniques, 5, p946. (Translation from Pribory i Tekhnika Eksperimenta 5, p 126. )
- (17) King, R.B., , Parnes, B. R., Davis, M.H. and Olsen, K. H., (1955), J. Opt. Soc. Am., 45, pp. 350-353.
- (18) King, R. B., (1948), Ap. J., 108, pp87-91.
- (19) Aller, L., Goldberg, L., and Muller, E. (1960), Supplement Ap. J., 5, pp lff.
- (20) Ostrovskii, Yu. I. and Penkin, N. P., (1958), Optika i Spektroskopiya, 5, 345-353.

- (21) Prokofjew, V.K., (1924), Trudy Gosudarstvenogo Opticheskogo Instituta (Leningrad), 3, pp 1-31.
- (22) Ismalov, I.I., and Filippov, A.N., (1933), Zhurnal Eksperimental'noi i Teoreticheskoi Fiziki, 3, pp524-525.
- (\* ) The last three papers are available in English translation: Optical Transition Probabilities. A Collection of Russian Articles, 1924-1960.  
US Dept. of Commerce, 1960.
- (23) Corliss, C. H. and Bozman, W. R. (1962), Experimental Transition Probabilities of Spectral Lines of Seventy Elements. (NBS Monograph #52.)
- (24) Hinnoy, F., and Kohn, H., J. Opt. Soc. Am. (1957) 47, 156.
- (25) Estabrook, F.B., (1951), Ap. J., ~~47, 156.~~ 113, 684-689.
- (26) Private communication of R. B. King to Leo Brewer, Letter, (1957).
- (27) Morris, J. P., Zellars, G. R., Payne, S. L., and Kipp, R. L., (1957), Bureau of Mines, Report of Investigations, 5364.
- (28) Moise, N., (1963), Thesis (Calif. Inst. of Tech. )
- (29) University of California at Berkely, Metallurgy Group, Minerals Research Lab., Inst of Engineering Research, Bulletin (Revised 1960).
- (30) Allen, C. W., and Asaad, A. S., (1957), Monthly Notices Roy. Astron. Soc., 117, 35 ff.
- (31) Allen, C.W., (1960), Monthly Notices Roy. Astron. Soc. 121, pp299-332.
- (32) Demtröder, W., (1962), Z. f. Physik, 166, 42.

## Appendix I

## Precision of Atomic Wavelength and f-value Measurements.

It is often remarked that although wavelengths of many thousands of atomic transitions are known to six or more significant figures, the f-values for these transitions are seldom known to better than one figure, if at all. Workers in the field of spectroscopy are confronted with this large difference in the precision of these two important quantities connected with a spectral transition. A few comments will be made here on the reasons for the difference.

Wavelengths can be measured experimentally with great accuracy because instruments have been built which can identify the wavelength of a light quanta with a high degree of accuracy and little ambiguity. Also, in atomic transitions, the natural width of a line is small compared with the wavelength of the line. Experimentally, the spectroscopist studies a statistical distribution function that describes the numbers of photons detected per wavelength interval at wavelengths around the line. The mean of the distribution is the wavelength of the line and is usually  $10^7$  times as big as the width of the distribution. If the experimenter wants to measure the strength of a line by counting photons, he has to count  $10^{14}$  photons to obtain approximately the same precision as can be obtained in measurement of the wavelength of one photon. Unfortunately, however, experimental difficulties have produced more uncertainties than this statistical limitation. In emission and absorption experiments, the major difficulty has been the determination of the density of the atomic states involved. This has been especially true in the case of high melting point metals and the case of ions. In lifetime measurements, the

problem has been the inability to handle accurately at high speed the small photon flux from weak concentrations of atoms or the problem of photon entrapment in dense concentrations. Recent developments in lifetime measurements, however, (32) exhibit estimated accuracy of 5%.

## Appendix II Photographs

Figure 13 is an interesting photograph of a cobalt beam. The beam is emitting light because of a hot cathode glow discharge formed at the crucible orifice. The photograph is taken with the camera at the side of the furnace with an ultra-violet passing filter in front of the lens. The glow appears blue-violet to the eye. The light beam used in absorption measurements passes from right to left as shown. In the production of the cobalt beam pictured, the tantalum furnace tube is at  $2200^{\circ}\text{K}$  and emits electrons thermionically. A high voltage transformer was connected between the furnace tube and the furnace framework (ground) and the pictured discharge occurred. The discharge draws about one ampere at about fifty volts and occurs only when the furnace is negative with respect to ground.

It was noticed that the initiation of the discharge reduced the equivalent width of an absorption line from the ground state by 30-40%, about the duty cycle of the discharge.

Measurements of the angle of the beam made from a similar photograph showed the angle to be the same as the angle calculated from the measured geometry.

Figure 14 is a photograph of the scanner carriage mounted on the spectrograph camera holder.

Figure 15 shows the furnace, the microbalance, and the vacuum pump input port. The lenses have been moved closer than usual to the center of the beam area. The vacuum enclosure has been removed to show the parts in their relative positions.

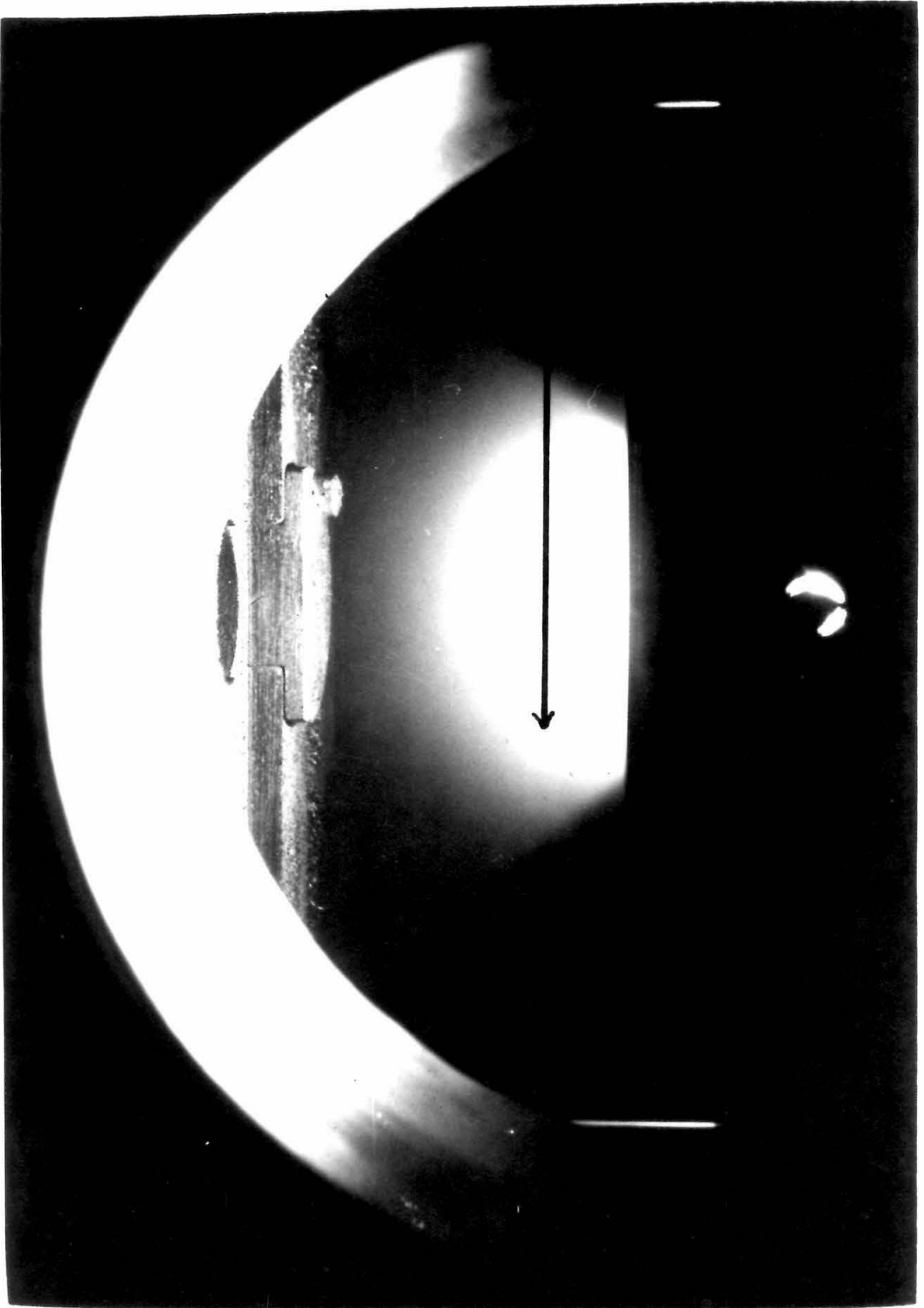


FIG. 13

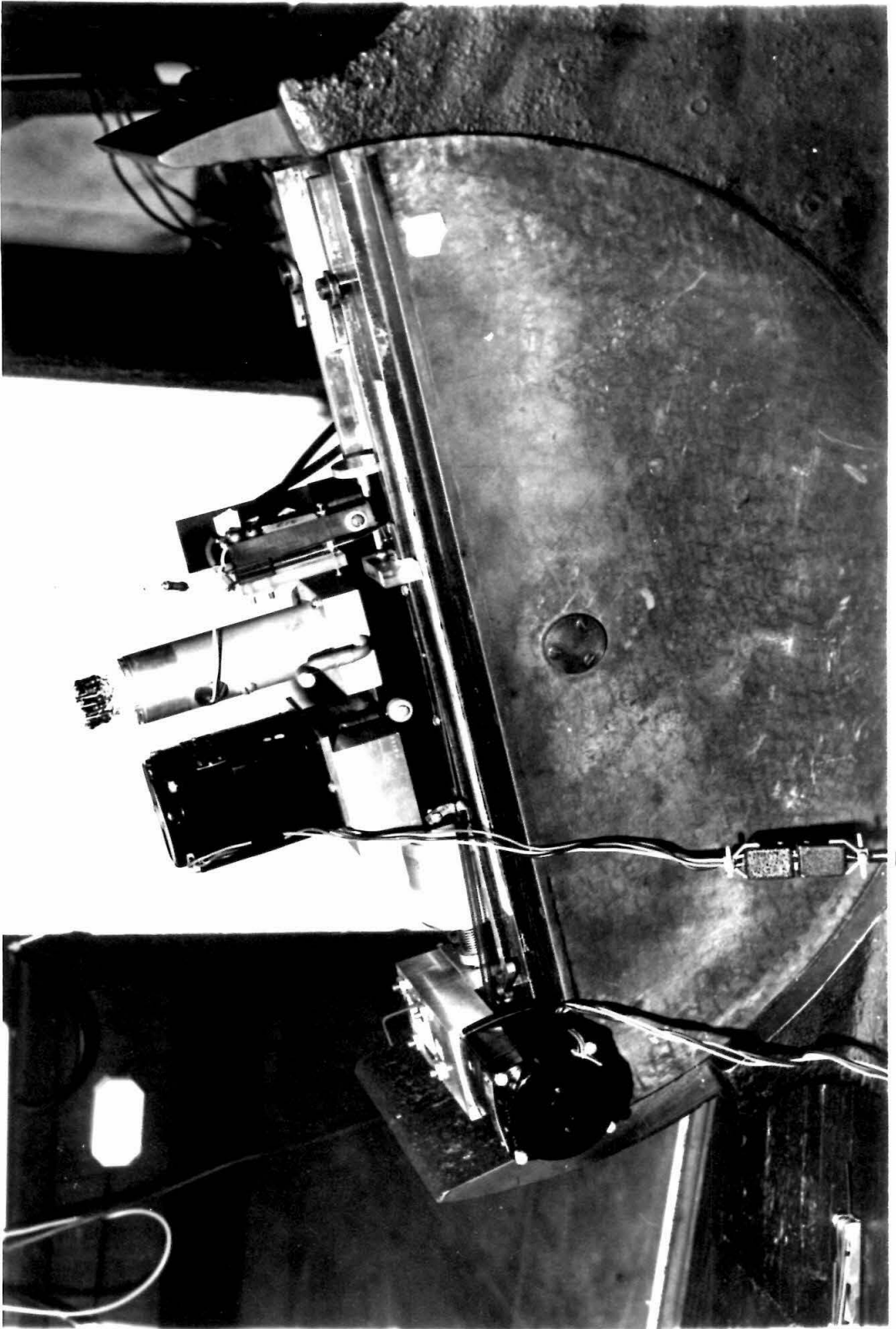


FIG. 14

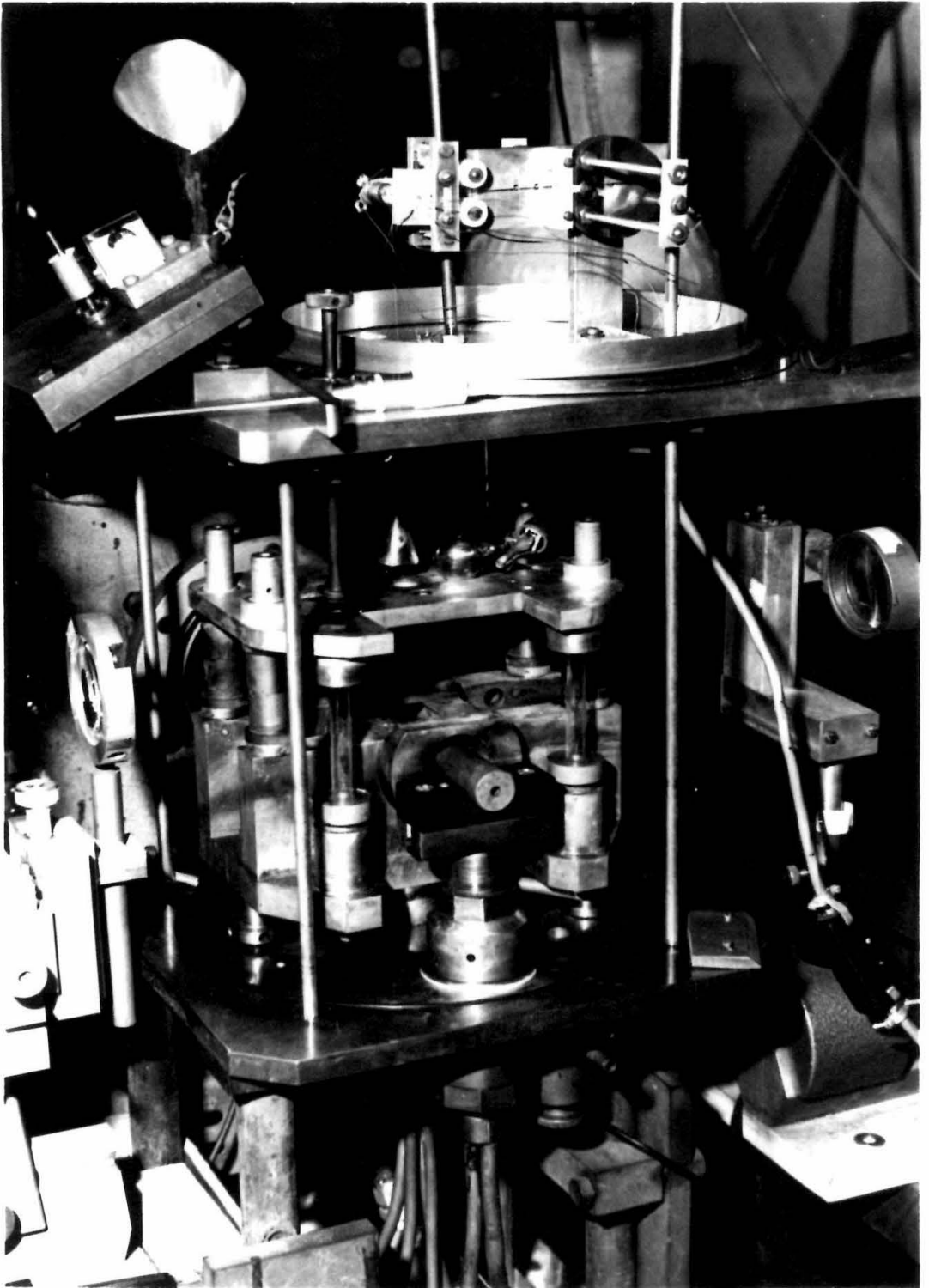


FIG. 15